PERGAMON

International Journal of Solids and Structures 36 (1999) 5425–5451

INTERNATIONAL JOURNAL OF SOLIDS and STRUCTURES

www.elsevier.com/locate/ijsolstr

A shell finite element for large strain elastoplasticity with anisotropies—Part II: Constitutive equations and numerical applications

B. Schieck[a], W.M. Smoleński[b], H. Stumpf[b,*]

[a] *Fachhochschule Lübeck, Fachbereich M + W, D-23562 Lübeck, Germany*
[b] *Lehrstuhl für Allgemeine Mechanik, Ruhr-Universität Bochum, D-44780 Bochum, Germany*

Received 5 January 1998; in revised form 5 August 1998

Abstract

An eight-node C^0 shell element for finite elastic–plastic deformations with anisotropies is developed. It combines the advantages of an isoparametric description of geometry and deformation, the application of tensors in Cartesian components, and a real and effective plane stress description with three displacement and three director degrees-of-freedom at each node. In Part I of the paper the shell theory including the kinematics, the variational principle, the application of Lagrange multipliers with their condensation on the element level and a comparative study of various assumed strain techniques were presented and the results of convergence tests given.

In this paper, we consider the constitutive equations for large elastic and large plastic strains accounting for initial and induced anisotropies and the corresponding thermodynamics. Then we investigate the return algorithm for finite strains and the implementation of the element procedure including stiffness matrix and residual force vector. Finally, we present the results of extended numerical applications and a comparison with FE solutions published in the literature, as far as such are available.

1. Introduction

According to the kinematics of finite elastoplasticity presented in Schieck and Stumpf (1995) and Part I of this paper the total deformation gradient can be decomposed into Lagrangian and Eulerian, respectively, elastic and plastic stretches and a uniquely defined rotation tensor. Correspondingly, the total stretch can be decomposed uniquely into Lagrangian and Eulerian, respectively, elastic and plastic stretches. From this result it follows that for the rate formulation

* Corresponding author. Tel.: 00 49 234 70 06 025; fax: 00 49 234 70 94 154; e-mail: stumpf@am.bi.ruhr-uni-bochum.de

0020-7683/99/$ - see front matter
PII: S0020-7683(98)00255-8

of the constitutive equations, we can choose either the time derivative within a Lagrangian description or the corotational rate formulation within the Eulerian picture, where the corotational rate is constructed with the spin of the uniquely defined rotation tensor. In Part I we also derived the kinematics of finite elastoplasticity for an additional reference configuration. To develop a shell finite element for large elastic and large plastic strains and arbitrary anisotropies we can then choose as first reference configuration the undeformed shell and as second reference configuration a flat rectangular plate, which enables us to apply the plane stress assumption for the shell element. As a basis for the derivation of the shell element a Lagrangian virtual work principle is formulated, where the transverse normality constraint and the condition of isochoric deformation are introduced by Lagrange multipliers, which can be condensed on the element level. Assumed strain techniques to avoid the membrane locking were proposed and compared with methods published in the literature.

This paper is organized as follows: in Section 2 we present the thermodynamically based elastic–plastic constitutive model for large elastic and large plastic strains with initial and induced anisotropies. In Section 3 the elastic–plastic return algorithm for finite strains is established and in Section 4 we consider the numerical implementation. In Section 5 a comprehensive set of numerical examples is provided. They illustrate the performance of the proposed eight-node shell finite element for a wide variety of engineering problems with the strain localization and necking of a plane specimen under tension, the elastic–plastic deformation of a plate with bending strain localization at the four corner zones, the elastic–plastic deformation of the Scordelis-Lo roof with bending strain localization in two zones of the shell and the elastic–plastic buckling of a cylinder under torsion exhibiting a significant influence of the ratio between kinematic and isotropic hardening.

2. Constitutive model

According to eqn [I(2.4)] (I refers to Part I) the total deformation gradient $\mathbf{F}$ can be decomposed multiplicatively into elastic and plastic Lagrangian $\mathbf{U}^e$, $\mathbf{U}^p$ and Eulerian $\mathbf{V}^e$, $\mathbf{V}^p$, respectively, stretches and a uniquely defined rotation tensor $\mathbf{Q}$:

$$\mathbf{F} = \mathbf{Q}\mathbf{U}^e\mathbf{U}^p = \mathbf{V}^e\mathbf{V}^p\mathbf{Q}, \quad \mathbf{Q} = \mathbf{R}^e\mathbf{R}^p, \tag{2.1}$$

with

$$\mathbf{U}^e := \mathbf{R}^{pT}\bar{\mathbf{U}}^e\mathbf{R}^p = \mathbf{Q}^T\mathbf{V}^e\mathbf{Q}, \quad \mathbf{V}^p = \mathbf{Q}\mathbf{U}^p\mathbf{Q}^T, \tag{2.2}$$

where $\mathbf{R}^e$, $\mathbf{R}^p$ are the elastic and plastic rotations following from the elastic and plastic deformation gradients $\mathbf{F}^e$, $\mathbf{F}^p$ by polar decompositions. The right and left total stretch tensors $\mathbf{U}$, $\mathbf{V}$, following from the polar decomposition of the total deformation gradient $\mathbf{F}$ can be decomposed into elastic and plastic stretches as follows

$$\mathbf{U} = \sqrt{\mathbf{F}^T\mathbf{F}} = \sqrt{\mathbf{U}^p\mathbf{U}^{e2}\mathbf{U}^p}, \quad \mathbf{V} = \sqrt{\mathbf{F}\mathbf{F}^T} = \sqrt{\mathbf{V}^e\mathbf{V}^{p2}\mathbf{V}^e}. \tag{2.3}$$

Solving $(2.3)_1$ with respect to $\mathbf{U}^e$ leads to the result that $\mathbf{U}^e$ is independent of the plastic rotation $\mathbf{R}^p$ or any additionally introduced plastic rotation $\mathbf{O}^p$. This proves the Lagrangian objectivity of $\mathbf{U}^e$. Analogously, solving $(2.3)_2$ with respect to $\mathbf{V}^p$ shows the independence of $\mathbf{V}^p$ from the plastic

rotation $\mathbf{R}^{\mathrm{p}}$ or any additionally introduced plastic rotation $\mathbf{O}^{\mathrm{p}}$. Therefore, $\mathbf{V}^{\mathrm{p}}$ is a Eulerian objective like $\mathbf{V}$ and $\mathbf{V}^{\mathrm{e}}$ (see also Ogden, 1984).

The eqns (2.2) can be interpreted as follows: the Lagrangian objective elastic stretch tensor $\mathbf{U}^{\mathrm{e}}$ is the pull-back with $\mathbf{Q}$ of the Eulerian objective elastic stretch tensor $\mathbf{V}^{\mathrm{e}}$ and the Eulerian objective plastic stretch tensor $\mathbf{V}^{\mathrm{p}}$ is the push-forward with $\mathbf{Q}$ of the Lagrangian plastic stretch tensor $\mathbf{U}^{\mathrm{p}}$. Therefore, to construct objective rates for $\mathbf{V}^{\mathrm{e}}$ and $\mathbf{V}^{\mathrm{p}}$ we use the spin $\boldsymbol{\Omega} = \dot{\mathbf{Q}}\mathbf{Q}^{\mathrm{T}}$ of the rotation tensor $\mathbf{Q}$ leading to a corotational rate or Lie-type derivative with respect to $\mathbf{Q}$:

$$\overset{\nabla}{\mathbf{V}}{}^{\mathrm{e}} := \mathbf{Q}\dot{\mathbf{U}}^{\mathrm{e}}\mathbf{Q}^{\mathrm{T}} = \mathbf{Q}\frac{\partial}{\partial t}(\mathbf{Q}^{\mathrm{T}}\mathbf{V}^{\mathrm{e}}\mathbf{Q})\mathbf{Q}^{\mathrm{T}} = \dot{\mathbf{V}}^{\mathrm{e}} - \boldsymbol{\Omega}\mathbf{V}^{\mathrm{e}} + \mathbf{V}^{\mathrm{e}}\boldsymbol{\Omega} \tag{2.4}$$

and

$$\overset{\nabla}{\mathbf{V}}{}^{\mathrm{p}} := \mathbf{Q}\dot{\mathbf{U}}^{\mathrm{p}}\mathbf{Q}^{\mathrm{T}} = \mathbf{Q}\frac{\partial}{\partial t}(\mathbf{Q}^{\mathrm{T}}\mathbf{V}^{\mathrm{p}}\mathbf{Q})\mathbf{Q}^{\mathrm{T}} = \dot{\mathbf{V}}^{\mathrm{p}} - \boldsymbol{\Omega}\mathbf{V}^{\mathrm{p}} + \mathbf{V}^{\mathrm{p}}\boldsymbol{\Omega} \tag{2.5}$$

with

$$\boldsymbol{\Omega} = \dot{\mathbf{Q}}\mathbf{Q}^{\mathrm{T}}. \tag{2.6}$$

The same objective corotational rate can be derived for all other Eulerian objective second-order tensors. For example, the rate of the Cauchy stress tensor $\boldsymbol{\sigma}$ with the back-rotated Cauchy stress tensor $\boldsymbol{\sigma}_0 = \mathbf{Q}^{\mathrm{T}}\boldsymbol{\sigma}\mathbf{Q}$ as a corresponding Lagrangian objective tensor takes the form

$$\overset{\nabla}{\boldsymbol{\sigma}} = \mathbf{Q}\dot{\boldsymbol{\sigma}}_0\mathbf{Q}^{\mathrm{T}} = \mathbf{Q}\frac{\partial}{\partial t}(\mathbf{Q}^{\mathrm{T}}\boldsymbol{\sigma}\mathbf{Q})\mathbf{Q}^{\mathrm{T}} = \dot{\boldsymbol{\sigma}} - \boldsymbol{\Omega}\boldsymbol{\sigma} + \boldsymbol{\sigma}\boldsymbol{\Omega}. \tag{2.7}$$

In order to determine $\boldsymbol{\Omega}$ we consider the spatial velocity gradient $\mathbf{l} = \dot{\mathbf{F}}\mathbf{F}^{-1}$:

$$\begin{aligned}\mathbf{l} = \dot{\mathbf{F}}\mathbf{F}^{-1} &= \dot{\mathbf{Q}}\mathbf{Q}^{\mathrm{T}} + \mathbf{Q}\dot{\mathbf{U}}^{\mathrm{e}}\mathbf{U}^{\mathrm{e}-1}\mathbf{Q}^{\mathrm{T}} + \mathbf{Q}\mathbf{U}^{\mathrm{e}}\dot{\mathbf{U}}^{\mathrm{p}}\mathbf{U}^{\mathrm{p}-1}\mathbf{U}^{\mathrm{e}-1}\mathbf{Q}^{\mathrm{T}} \\ &= \boldsymbol{\Omega} + \overset{\nabla}{\mathbf{V}}{}^{\mathrm{e}}\mathbf{V}^{\mathrm{e}-1} + \mathbf{V}^{\mathrm{e}}\overset{\nabla}{\mathbf{V}}{}^{\mathrm{p}}\mathbf{V}^{\mathrm{p}-1}\mathbf{V}^{\mathrm{e}-1}.\end{aligned} \tag{2.8}$$

The additive decomposition of $\mathbf{l}$ into symmetric and skew-symmetric parts yields

$$\mathbf{l} = \mathbf{d} + \mathbf{w} = \mathbf{d}^{\mathrm{e}} + \mathbf{d}^{\mathrm{p}} + \mathbf{w}^{\mathrm{e}} + \mathbf{w}^{\mathrm{p}} + \boldsymbol{\Omega}, \tag{2.9}$$

where

$$\mathbf{d} = \tfrac{1}{2}(\mathbf{l} + \mathbf{l}^{\mathrm{T}}) = \mathbf{d}^{\mathrm{e}} + \mathbf{d}^{\mathrm{p}}, \tag{2.10}$$

$$\mathbf{d}^{\mathrm{e}} = \tfrac{1}{2}(\overset{\nabla}{\mathbf{V}}{}^{\mathrm{e}}\mathbf{V}^{\mathrm{e}-1} + \mathbf{V}^{\mathrm{e}-1}\overset{\nabla}{\mathbf{V}}{}^{\mathrm{e}}), \tag{2.11}$$

$$\mathbf{d}^{\mathrm{p}} = \tfrac{1}{2}(\mathbf{V}^{\mathrm{e}}\overset{\nabla}{\mathbf{V}}{}^{\mathrm{p}}\mathbf{V}^{\mathrm{p}-1}\mathbf{V}^{\mathrm{e}-1} + \mathbf{V}^{\mathrm{e}-1}\mathbf{V}^{\mathrm{p}-1}\overset{\nabla}{\mathbf{V}}{}^{\mathrm{p}}\mathbf{V}^{\mathrm{e}}) \tag{2.12}$$

are the total, elastic and plastic deformation rates, respectively, and

$$\mathbf{w} = \tfrac{1}{2}(\mathbf{l} - \mathbf{l}^{\mathrm{T}}) = \boldsymbol{\Omega} + \mathbf{w}^{\mathrm{e}} + \mathbf{w}^{\mathrm{p}}, \tag{2.13}$$

$$\mathbf{w}^{e} = \tfrac{1}{2}(\overset{\nabla}{\mathbf{V}}{}^{e}\mathbf{V}^{e-1} - \mathbf{V}^{e-1}\overset{\nabla}{\mathbf{V}}{}^{e}), \tag{2.14}$$

$$\mathbf{w}^{p} = \tfrac{1}{2}(\mathbf{V}^{e}\overset{\nabla}{\mathbf{V}}{}^{p}\mathbf{V}^{p-1}\mathbf{V}^{e-1} - \mathbf{V}^{e-1}\mathbf{V}^{p-1}\overset{\nabla}{\mathbf{V}}{}^{p}\mathbf{V}^{e}) \tag{2.15}$$

are the total (usually called 'material'), elastic and plastic spins. The spin $\boldsymbol{\Omega}$ of the rotation tensor $\mathbf{Q}$ is then obtained as

$$\boldsymbol{\Omega} = \mathbf{w} - \mathbf{w}^{e} - \mathbf{w}^{p}. \tag{2.16}$$

A detailed discussion of this kinematical concept and several numerical examples for elastic and plastic deformations with various magnitudes were given in Schieck and Stumpf (1995). Within this concept the elastic deformation rate $\mathbf{d}^{e}$ is a linear function of the rate of the elastic stretch $\overset{\nabla}{\mathbf{V}}{}^{e}$ and the plastic deformation rate $\mathbf{d}^{p}$ is a linear function of the rate of the plastic stretch $\overset{\nabla}{\mathbf{V}}{}^{p}$. The result is a formally simple structure of the thermodynamically based constitutive equations, which are, therefore, easily accessible to engineers.

In the most general case, the free energy ψ per unit mass depends on the elastic stretch $\mathbf{V}^{e}$, the plastic stretch $\mathbf{V}^{p}$ including its history, a set $\mathscr{a}$ of initial anisotropy tensors and the absolute temperature θ. In the back-rotated configuration (the actual configuration back-rotated with $\mathbf{Q}$) with Lagrangian objective variables it depends on the elastic stretch $\mathbf{U}^{e}$, the plastic stretch $\mathbf{U}^{p}$ including its history, a set $\mathscr{A}$ of the back-rotated initial anisotropy tensors (e.g. second-order tensors $\mathbf{A} \in \mathscr{A}$ corresponding to $\mathbf{a} = \mathbf{Q}\mathbf{A}\mathbf{Q}^{T} \in \mathscr{a}$) and the absolute temperature θ. Therefore, we can postulate a free energy of the form

$$\psi = \psi(\mathbf{V}^{e}, \mathbf{V}^{p}, \mathscr{a}, \theta) = \psi(\mathbf{U}^{e}, \mathbf{U}^{p}, \mathscr{A}, \theta). \tag{2.17}$$

However, the free energy does not depend on actual anisotropy tensors as independent variables, because one can show that their rates are expressible through the rates of the independent variables in eqn (2.17). One should also note that the free energy is a potential only with respect to the elastic stretch, whereas its dependence on the plastic stretch may be strongly path-dependent.

Analogously, the yield function ϕ for rate-insensitive plasticity depends on the same set of free variables,

$$\phi = \phi(\mathbf{V}^{e}, \mathbf{V}^{p}, \mathscr{a}, \theta) = \phi(\mathbf{U}^{e}, \mathbf{U}^{p}, \mathscr{A}, \theta) \begin{cases} = 0 \Leftrightarrow \text{yielding} \\ < 0 \Leftrightarrow \text{no yielding} \end{cases}. \tag{2.18}$$

Alternative formulations for the yield function using kinetic instead of kinematic variables will be considered later.

From $(2.17)_2$ the rate of the free energy follows as

$$\dot{\psi} = \frac{\partial \psi}{\partial \mathbf{U}^{e}} \cdot \dot{\mathbf{U}}^{e} + \frac{\partial \psi}{\partial \mathbf{U}^{p}} \cdot \dot{\mathbf{U}}^{p} + \frac{\partial \psi}{\partial \theta}\dot{\theta}. \tag{2.19}$$

If the free energy depends on plastic anisotropies $\mathscr{A}^{p}$ the derivative $\partial\psi/\partial\mathbf{U}^{p}$ must be calculated as $\partial\psi/\partial\mathbf{U}^{p} = \partial\psi/\partial\mathbf{U}^{p}|_{\mathscr{A}^{p}=\text{const.}} + \partial\psi/\partial\mathscr{A}^{p}|_{\mathbf{U}^{p}=\text{const.}} \cdot \partial\mathscr{A}^{p}/\partial\mathbf{U}^{p}$, using the evolution law for the plastic anisotropies. Then the plastic anisotropies do not appear in eqn (2.17) as independent variables. However, if one treats them as independent variables, one can derive the evolution law for them

from the corresponding associated flow rule, which shows that the plastic anisotropies do not appear in the free energy as independent variables. By push-forward of eqn (2.19) with the rotation tensor $\mathbf{Q}$ one gets

$$\dot{\psi} = \frac{\partial \psi}{\partial \mathbf{V}^{\mathrm{e}}} \cdot \overset{\nabla}{\mathbf{V}}{}^{\mathrm{e}} + \frac{\partial \psi}{\partial \mathbf{V}^{\mathrm{p}}} \cdot \overset{\nabla}{\mathbf{V}}{}^{\mathrm{p}} + \frac{\partial \psi}{\partial \theta} \dot{\theta}. \tag{2.20}$$

Using computer algebra (e.g. Mathematics, Maple, etc.) one can solve eqns (2.11) and (2.12) with respect to $\overset{\nabla}{\mathbf{V}}{}^{\mathrm{e}}$ and $\overset{\nabla}{\mathbf{V}}{}^{\mathrm{p}}$ obtaining them as linear functions of $\mathbf{d}^{\mathrm{e}}$ and $\mathbf{d}^{\mathrm{p}}$. These functions will be denoted by $\partial \overset{\nabla}{\mathbf{V}}{}^{\mathrm{e}} / \partial \mathbf{d}^{\mathrm{e}}$ and $\partial \overset{\nabla}{\mathbf{V}}{}^{\mathrm{p}} / \partial \mathbf{d}^{\mathrm{p}}$ in the following considerations. They allow us to rewrite eqn (2.20) as

$$\dot{\psi} = \frac{\partial \dot{\psi}}{\partial \mathbf{d}^{\mathrm{e}}} \cdot \mathbf{d}^{\mathrm{e}} + \frac{\partial \dot{\psi}}{\partial \mathbf{d}^{\mathrm{p}}} \cdot \mathbf{d}^{\mathrm{p}} + \frac{\partial \psi}{\partial \theta} \dot{\theta}, \tag{2.21}$$

where $\partial \dot{\psi} / \partial \mathbf{d}^{\mathrm{e}}$ and $\partial \dot{\psi} / \partial \mathbf{d}^{\mathrm{p}}$ stand for

$$\frac{\partial \dot{\psi}}{\partial \mathbf{d}^{\mathrm{e}}} = \frac{\partial \psi}{\partial \mathbf{V}^{\mathrm{e}}} \cdot \frac{\partial \overset{\nabla}{\mathbf{V}}{}^{\mathrm{e}}}{\partial \mathbf{d}^{\mathrm{e}}} \quad \text{and} \quad \frac{\partial \dot{\psi}}{\partial \mathbf{d}^{\mathrm{p}}} = \frac{\partial \psi}{\partial \mathbf{V}^{\mathrm{p}}} \cdot \frac{\partial \overset{\nabla}{\mathbf{V}}{}^{\mathrm{p}}}{\partial \mathbf{d}^{\mathrm{p}}}. \tag{2.22}$$

Inserting eqn (2.21) into the localized Clausius–Duhem inequality

$$\rho(\eta \dot{\theta} + \dot{\psi}) - \boldsymbol{\sigma} \cdot \mathbf{d} + \frac{1}{\theta} \nabla \theta \cdot \mathbf{q} \leqslant 0 \tag{2.23}$$

results in

$$\rho \left(\eta \dot{\theta} + \frac{\partial \dot{\psi}}{\partial \mathbf{d}^{\mathrm{e}}} \cdot \mathbf{d}^{\mathrm{e}} + \frac{\partial \dot{\psi}}{\partial \mathbf{d}^{\mathrm{p}}} \cdot \mathbf{d}^{\mathrm{p}} + \frac{\partial \psi}{\partial \theta} \dot{\theta} \right) - \boldsymbol{\sigma} \cdot (\mathbf{d}^{\mathrm{e}} + \mathbf{d}^{\mathrm{p}}) + \frac{1}{\theta} \nabla \theta \cdot \mathbf{q} \leqslant 0. \tag{2.24}$$

In these equations ρ denotes the actual mass density, η the entropy per unit mass, $\boldsymbol{\sigma}$ the (true) Cauchy stress tensor, $\nabla(\cdot)$ the gradient of $(\cdot)$ in the actual configuration and $\mathbf{q}$ the heat flux. Following now the common interpretation given in more detailed form in Le and Stumpf (1993) and Acharya and Shawki (1996), one obtains

$$\eta = -\frac{\partial \psi}{\partial \theta}, \quad \text{(entropy)} \tag{2.25}$$

$$-\mathbf{q} \cdot \nabla \theta \geqslant 0, \quad \text{(direction of heat flux)} \tag{2.26}$$

$$\boldsymbol{\sigma} = \rho \frac{\partial \dot{\psi}}{\partial \mathbf{d}^{\mathrm{e}}}, \quad \text{(definition of true stress)} \tag{2.27}$$

$$D^{\mathrm{p}} := \left(\boldsymbol{\sigma} - \rho \frac{\partial \dot{\psi}}{\partial \mathbf{d}^{\mathrm{p}}} \right) \cdot \mathbf{d}^{\mathrm{p}} \geqslant 0 \quad \text{(plastic dissipation)}. \tag{2.28}$$

The plastic dissipation D^{p} according to (2.28) suggests to define a 'plastic stress'

$$\boldsymbol{\sigma}^{\mathrm{p}} := \boldsymbol{\sigma} - \rho \frac{\partial \psi}{\partial \mathbf{d}^{\mathrm{p}}} = \boldsymbol{\sigma} - \frac{\rho}{\rho_0} \boldsymbol{\alpha} \tag{2.29}$$

power-conjugate to $\mathbf{d}^{\mathrm{p}}$, where

$$\boldsymbol{\alpha} := \rho_0 \frac{\partial \dot{\psi}}{\partial \mathbf{d}^{\mathrm{p}}} \tag{2.30}$$

is an 'internal stress', to be interpreted below as the back-stress in the yield condition, and ρ_0 denotes the mass density in the reference configuration. Comparing the plastic dissipation (2.28) with the plastic dissipation resulting from theories with Lie-derivatives (e.g. Le and Stumpf, 1993 or Miehe, 1998a), one can prove their equivalence.

According to common arguments (for small strains Sedow, 1972, gave an extended derivation), the yield function ϕ should be formulated using the 'plastic stress' of the plastic dissipation inequality, if ϕ has to be formulated in the stress space. If, analogously to the free energy ψ, the yield function ϕ is referred to the unit mass, it is reasonable to use Kirchhoff stress tensors

$$\boldsymbol{\tau} = \frac{\rho_0}{\rho} \boldsymbol{\sigma}, \quad \boldsymbol{\tau}^{\mathrm{p}} = \frac{\rho_0}{\rho} \boldsymbol{\sigma}^{\mathrm{p}} = \boldsymbol{\tau} - \boldsymbol{\alpha}. \tag{2.31}$$

Additionally, in most cases the yield function ϕ should depend on a set $\mathscr{C}$ of internal variables (of various tensorial types) that depend on the plastic stretch $\mathbf{V}^{\mathrm{p}}$ including its history and on the set a of initial anisotropies [according to the remarks below eqn (2.19), deformation-dependent (e.g. plastic) anisotropies are not independent variables]. Accounting also for the temperature θ, this results in

$$\phi = \phi(\boldsymbol{\tau}^{\mathrm{p}}, \mathscr{C}, \theta) = \phi(\boldsymbol{\tau} - \boldsymbol{\alpha}, \mathscr{C}, \theta) \begin{cases} = 0 \Leftrightarrow \text{yielding} \\ < 0 \Leftrightarrow \text{no yielding} \end{cases}. \tag{2.32}$$

The yield function ϕ can also be formulated in terms of variables referred to the back-rotated, Lagrangian objective configuration, using back-rotated stress tensors $\boldsymbol{\tau}_0 = \mathbf{Q}^{\mathrm{T}} \boldsymbol{\tau} \mathbf{Q}$, $\boldsymbol{\alpha}_0 = \mathbf{Q}^{\mathrm{T}} \boldsymbol{\alpha} \mathbf{Q}$, $\boldsymbol{\tau}_0^{\mathrm{p}} = \mathbf{Q}^{\mathrm{T}} \boldsymbol{\tau}^{\mathrm{p}} \mathbf{Q}$ and the set $\mathscr{B}$ of back-rotated internal variables depending on the plastic deformation $\mathbf{U}^{\mathrm{p}}$ and the set $\mathscr{A}$ of initial anisotropies:

$$\phi = \phi(\boldsymbol{\tau}_0^{\mathrm{p}}, \mathscr{B}, \theta) = \phi(\boldsymbol{\tau}_0 - \boldsymbol{\alpha}_0, \mathscr{B}, \theta) \begin{cases} = 0 \Leftrightarrow \text{yielding} \\ < 0 \Leftrightarrow \text{no yielding} \end{cases}. \tag{2.33}$$

The formulae (2.32) and (2.33) of the yield function are equivalent to (2.18), because the sets of independent parameters in these formulations can be transformed one to the other.

The associated flow rule is then obtained from the principle of maximum plastic dissipation as

$$\mathbf{d}^{\mathrm{p}} = \dot{\lambda} \frac{\partial \phi}{\partial \boldsymbol{\tau}^{\mathrm{p}}} = \dot{\lambda} \frac{\partial \phi}{\partial \boldsymbol{\tau}}, \quad \dot{\lambda} \geqslant 0, \quad \dot{\lambda} \phi = 0. \tag{2.34}$$

In the present paper we assume that the elastic and plastic contributions to the free energy are uncoupled, i.e.

$$\frac{\partial^2\psi}{\partial\mathbf{U}^e\otimes\partial\mathbf{U}^p}=\frac{\partial^2\psi}{\partial\mathbf{V}^e\otimes\partial\mathbf{V}^p}=\mathbf{0}, \tag{2.35}$$

which means that we assume isotropy in the elastic range of deformation. This holds approximately for many polycrystalline materials such as most metal alloys, for which Young's moduli are known to be macroscopically constant and independent of the deformation history. Equation (2.35) is equivalent to the assumption that the Kirchhoff stress depends only on the elastic deformation,

$$\boldsymbol{\tau}=\boldsymbol{\tau}(\mathbf{V}^e)\quad\text{or}\ \boldsymbol{\tau}_0=\mathbf{Q}^T\boldsymbol{\tau}\mathbf{Q}=\boldsymbol{\tau}_0(\mathbf{U}^e). \tag{2.36}$$

From the above assumptions, from eqn (2.27) and the definition of the corotational rate (2.4)–(2.7), one obtains the incremental elastic constitutive equations in the Eulerian and Langrangian picture

$$\overset{\nabla}{\boldsymbol{\tau}}=\mathbb{C}^e\cdot\mathbf{d}^e,\quad\dot{\boldsymbol{\tau}}_0=\mathbb{C}_0^e\cdot\mathbf{D}^e, \tag{2.37}$$

where

$$\mathbb{C}^e=\rho_0\left(\frac{\partial\overset{\nabla}{\mathbf{V}}{}^e}{\partial\mathbf{d}^e}\right)^T\cdot\frac{\partial^2\psi}{\partial\mathbf{V}^e\otimes\partial\mathbf{V}^e}\cdot\frac{\partial\overset{\nabla}{\mathbf{V}}{}^e}{\partial\mathbf{d}^e},\quad\mathbb{C}_0^e=\rho_0\left(\frac{\partial\dot{\mathbf{U}}^e}{\partial\mathbf{D}^e}\right)^T\cdot\frac{\partial^2\psi}{\partial\mathbf{U}^e\otimes\partial\mathbf{U}^e}\cdot\frac{\partial\dot{\mathbf{U}}^e}{\partial\mathbf{D}^e} \tag{2.38}$$

are the tangent elasticity tensors of fourth-order and

$$\mathbf{D}^e=\mathbf{Q}^T\mathbf{d}^e\mathbf{Q}=\tfrac{1}{2}(\dot{\mathbf{U}}^e\mathbf{U}^{e-1}+\mathbf{U}^{e-1}\dot{\mathbf{U}}^e) \tag{2.39}$$

is the back-rotated elastic deformation rate. With ρ_0 we denote the mass density in the undeformed configuration and with $\cdot$ the scalar product of tensors with double contraction of indices, if index notation is applied. For large elastic strains the tangent elasticity tensors $\mathbb{C}^e$ and $\mathbb{C}_0^e$ according to (2.38) depend on the elastic stretch tensors $\mathbf{V}^e$ and $\mathbf{U}^e$, respectively.

Introducing the consistent elastic–plastic tangent operators $\mathbb{C}^{ep}$ and $\mathbb{C}_0^{ep}$, the elastic–plastic rate constitutive equations are obtained in the actual configuration as

$$\overset{\nabla}{\boldsymbol{\tau}}=\mathbb{C}^{ep}\cdot\mathbf{d}, \tag{2.40}$$

and in the back-rotated configuration

$$\dot{\boldsymbol{\tau}}_0=\mathbb{C}_0^{ep}\cdot\mathbf{D}, \tag{2.41}$$

where in the latter case

$$\mathbf{D}=\mathbf{Q}^T\mathbf{d}\mathbf{Q}=\mathbf{D}^e+\mathbf{D}^p, \tag{2.42}$$

$$\mathbf{D}^e=\mathbf{Q}^T\mathbf{d}^e\mathbf{Q}=\tfrac{1}{2}(\dot{\mathbf{U}}^e\mathbf{U}^{e-1}+\mathbf{U}^{e-1}\dot{\mathbf{U}}^e),$$

$$\mathbf{D}^p=\mathbf{Q}^T\mathbf{d}^p\mathbf{Q}=\tfrac{1}{2}(\mathbf{U}^e\dot{\mathbf{U}}^p\mathbf{U}^{p-1}\mathbf{U}^{e-1}+\mathbf{U}^{e-1}\mathbf{U}^{p-1}\dot{\mathbf{U}}^p\mathbf{U}^e) \tag{2.43}$$

are the back-rotated total, elastic and plastic deformation rates. The tangent operators $\mathbb{C}^{ep}$ and $\mathbb{C}_0^{ep}$ are derived from the consistency condition $\dot{\phi}=0$, the flow rule (2.34) and the incremental elastic constitutive equations (2.37) as

$$\mathbb{C}^{ep} = \mathbb{C}^{e} - \frac{\mathbb{C}^{e} \cdot \dfrac{\partial \phi}{\partial \boldsymbol{\tau}} \otimes \dfrac{\partial \phi}{\partial \boldsymbol{\tau}} \cdot \mathbb{C}^{e}}{\dfrac{\partial \phi}{\partial \boldsymbol{\tau}} \cdot \mathbb{C}^{e} \cdot \dfrac{\partial \phi}{\partial \boldsymbol{\tau}} - \dfrac{\partial \dot{\phi}}{\partial \mathbf{d}^{p}} \cdot \dfrac{\partial \phi}{\partial \boldsymbol{\tau}}}, \tag{2.44}$$

$$\mathbb{C}_0^{ep} = \mathbb{C}_0^{e} - \frac{\mathbb{C}_0^{e} \cdot \dfrac{\partial \phi}{\partial \boldsymbol{\tau}_0} \otimes \dfrac{\partial \phi}{\partial \boldsymbol{\tau}_0} \cdot \mathbb{C}_0^{e}}{\dfrac{\partial \phi}{\partial \boldsymbol{\tau}_0} \cdot \mathbb{C}_0^{e} \cdot \dfrac{\partial \phi}{\partial \boldsymbol{\tau}_0} - \dfrac{\partial \dot{\phi}}{\partial \mathbf{D}^{p}} \cdot \dfrac{\partial \phi}{\partial \boldsymbol{\tau}_0}}. \tag{2.45}$$

Due to eqn (2.32), we have

$$\frac{\partial \phi}{\partial \boldsymbol{\tau}} = \frac{\partial \phi}{\partial \boldsymbol{\tau}^{p}}, \quad \frac{\partial \phi}{\partial \boldsymbol{\tau}_0} = \frac{\partial \phi}{\partial \boldsymbol{\tau}_0^{p}} \tag{2.46}$$

and

$$\frac{\partial \dot{\phi}}{\partial \mathbf{d}^{p}} = \frac{\partial \phi}{\partial \boldsymbol{\alpha}} \cdot \frac{\partial \dot{\boldsymbol{\alpha}}}{\partial \mathbf{d}^{p}} + \sum_i \frac{\partial \phi}{\partial b_i} \frac{\partial \dot{b}_i}{\partial \mathbf{d}^{p}}, \quad \frac{\partial \phi}{\partial \mathbf{D}^{p}} = \frac{\partial \phi}{\partial \boldsymbol{\alpha}_0} \cdot \frac{\partial \dot{\boldsymbol{\alpha}}_0}{\partial \mathbf{D}^{p}} + \sum_i \frac{\partial \phi}{\partial B_i} \frac{\partial \dot{B}_i}{\partial \mathbf{D}^{p}}, \tag{2.47}$$

where b_i, B_i are elements of the sets $\mathscr{C}$ and $\mathscr{B}$ of internal variables depending on $\mathbf{V}^{p}$ and $\mathbf{U}^{p}$, respectively. In the case of von Mises yield condition with combined isotropic and kinematic hardening and fully three-dimensional description, the denominator of eqns (2.44), (2.45) become $2G+h$, where G is the shear modulus and h the total hardening modulus. In the same case but for plane stress, only $-\partial \dot{\phi}/\partial \mathbf{d}^{p} \cdot \partial \phi/\partial \boldsymbol{\tau}$ or $-\partial \dot{\phi}/\partial \mathbf{D}^{p} \cdot \partial \phi/\partial \boldsymbol{\tau}_0$ in the denominators of (2.44), (2.45) can be replaced by $+h$.

In the numerical examples the isotropic elastic constitutive equation is chosen according to Anand (1979, 1986) as

$$\boldsymbol{\tau} = \mathbb{C} \cdot \ln(\mathbf{V}^{e}), \quad \boldsymbol{\tau}_0 = \mathbb{C} \cdot \ln(\mathbf{U}^{e}), \quad \mathbb{C} = \text{const.} \tag{2.48}$$

Within moderately large elastic strains $\|\ln(\mathbf{V}^{e})\| \leqslant 10\%$ one can show that within a relative error of about 1% we have

$$\mathbb{C}^{e} = \mathbb{C}_0^{e} \approx \mathbb{C}. \tag{2.49}$$

For larger elastic strains one has to calculate

$$\mathbb{C}^{e} = \mathbb{C} \cdot \frac{\partial (\ln \mathbf{V}^{e})^{\nabla}}{\partial \mathbf{d}^{e}}, \quad \mathbb{C}_0^{e} = \mathbb{C} \cdot \frac{\partial (\ln \mathbf{U}^{e})^{\cdot}}{\partial \mathbf{D}^{e}} \tag{2.50}$$

exactly. Details of this analysis can be found in Section 6 and in the Appendix of Schieck and Stumpf (1995).

In the numerical examples of this paper we have taken von Mises yield condition and associated flow rule with combined isotropic and kinematic hardening. For plane stress one obtains in terms of physical components

$$\phi = \sqrt{\operatorname{dev}(\boldsymbol{\tau} - \boldsymbol{\alpha}) \cdot \operatorname{dev}(\boldsymbol{\tau} - \boldsymbol{\alpha})} - \sqrt{\tfrac{2}{3}}\tau_y$$

$$= \sqrt{\tfrac{2}{3}}\Big(\sqrt{(\tau_{11}-\alpha_{11})^2+(\tau_{22}-\alpha_{22})^2-(\tau_{11}-\alpha_{11})(\tau_{22}-\alpha_{22})}$$
$$\overline{-(\tau_{11}+\tau_{22}-2\alpha_{11}-2\alpha_{22})(\alpha_{11}+\alpha_{22})+3(\tau_{12}-\alpha_{12})^2}-\tau_y\Big) \leqslant 0, \tag{2.51}$$

where τ_y is the uniaxial average yield stress. Of course, in eqn (2.51) components of $\boldsymbol{\tau}_0$ and $\boldsymbol{\alpha}_0$ can be used instead of $\boldsymbol{\tau}$ and $\boldsymbol{\alpha}$. The isotropic and kinematic hardening rules are chosen as

$$\dot{\tau}_y = \sqrt{\tfrac{3}{2}}(1-\beta)h\|\mathbf{d}^{\mathrm{p}}\| \quad \text{and} \quad \overset{\nabla}{\boldsymbol{\alpha}} = \beta h\mathbf{d}^{\mathrm{p}}, \tag{2.52}$$

where β is the ratio of kinematic hardening,

$$h = \frac{2}{3}\frac{EE_{\mathrm{T}}}{E-E_{\mathrm{T}}} \tag{2.53}$$

is the hardening modulus with E as Young's modulus and E_{T} as tangent modulus, and $\|\mathbf{d}^{\mathrm{p}}\| = \sqrt{(d^{\mathrm{p}}_{11})^2+(d^{\mathrm{p}}_{22})^2+2(d^{\mathrm{p}}_{12})^2+(d^{\mathrm{p}}_{11}+d^{\mathrm{p}}_{22})^2} = \|\mathbf{D}^{\mathrm{p}}\|$ is the norm of $\mathbf{d}^{\mathrm{p}}$ or $\mathbf{D}^{\mathrm{p}}$ calculated in the three-dimensional space.

The constitutive equations can be formulated analogously also in the back-rotated configuration defined by $\mathbf{Q}_{\mathrm{R}}$ according to eqn [I(2.12)$_3$]. There, $\mathbf{Q}_{\mathrm{R}}$ is the composition of the rotation $\mathbf{Q}$ due to eqn (2.3) and the rotation of the mapping from the fictitious flat Cartesian reference configuration into the undeformed configuration. In Fig. 2I, this back-rotated configuration is depicted as $\tilde{\mathscr{B}}_*$. Using $\mathbf{U}^{\mathrm{e}}_{\mathrm{R}}$ and $\mathbf{U}^{\mathrm{p}}_{\mathrm{R}}$ due to eqns [I(2.12)$_{1,2}$], eqns (2.37)$_2$, (2.39), (2.41)–(2.43), (2.45) and (2.48) lead to

$$\dot{\boldsymbol{\tau}}_{\mathrm{R}} = \mathbb{C}^{\mathrm{e}}_{\mathrm{R}}\mathbf{D}^{\mathrm{e}}_{\mathrm{R}} = \mathbb{C}^{\mathrm{ep}}_{\mathrm{R}}\cdot\mathbf{D}_{\mathrm{R}}, \tag{2.55}$$

$$\mathbf{D}_{\mathrm{R}} = \mathbf{Q}^{\mathrm{T}}_{\mathrm{R}}\mathbf{d}\mathbf{Q}_{\mathrm{R}} = \mathbf{D}^{\mathrm{e}}_{\mathrm{R}}+\mathbf{D}^{\mathrm{p}}_{\mathrm{R}}, \tag{2.56}$$

$$\mathbf{D}^{\mathrm{e}}_{\mathrm{R}} = \mathbf{Q}^{\mathrm{T}}_{\mathrm{R}}\mathbf{d}^{\mathrm{e}}\mathbf{Q}_{\mathrm{R}} = \tfrac{1}{2}(\dot{\mathbf{U}}^{\mathrm{e}}_{\mathrm{R}}\mathbf{U}^{\mathrm{e}-1}_{\mathrm{R}}+\mathbf{U}^{\mathrm{e}-1}_{\mathrm{R}}\dot{\mathbf{U}}^{\mathrm{e}}_{\mathrm{R}}), \tag{2.57}$$

$$\mathbf{D}^{\mathrm{p}}_{\mathrm{R}} = \mathbf{Q}^{\mathrm{T}}_{\mathrm{R}}\mathbf{d}^{\mathrm{p}}\mathbf{Q}_{\mathrm{R}} = \tfrac{1}{2}(\mathbf{U}^{\mathrm{e}}_{\mathrm{R}}\dot{\mathbf{U}}^{\mathrm{p}}_{\mathrm{R}}\mathbf{U}^{\mathrm{p}-1}_{\mathrm{R}}\mathbf{U}^{\mathrm{e}-1}_{\mathrm{R}}+\mathbf{U}^{\mathrm{e}-1}_{\mathrm{R}}\mathbf{U}^{\mathrm{p}-1}_{\mathrm{R}}\dot{\mathbf{U}}^{\mathrm{p}}_{\mathrm{R}}\mathbf{U}^{\mathrm{e}}_{\mathrm{R}}), \tag{2.58}$$

$$\boldsymbol{\tau}_{\mathrm{R}} = \mathbb{C}\ln(\mathbf{U}^{\mathrm{e}}_{\mathrm{R}}), \tag{2.59}$$

where

$$\mathbb{C}^{\mathrm{ep}}_{\mathrm{R}} = \mathbb{C}^{\mathrm{e}}_{\mathrm{R}} - \frac{\mathbb{C}^{\mathrm{e}}_{\mathrm{R}}\cdot\dfrac{\partial\phi}{\partial\boldsymbol{\tau}_{\mathrm{R}}}\otimes\dfrac{\partial\phi}{\partial\boldsymbol{\tau}_{\mathrm{R}}}\cdot\mathbb{C}^{\mathrm{e}}_{\mathrm{R}}}{\dfrac{\partial\phi}{\partial\boldsymbol{\tau}_{\mathrm{R}}}\cdot\mathbb{C}^{\mathrm{e}}_{\mathrm{R}}\cdot\dfrac{\partial\phi}{\partial\boldsymbol{\tau}_{\mathrm{R}}}-\dfrac{\partial\dot{\phi}}{\partial\mathbf{D}^{\mathrm{p}}_{\mathrm{R}}}\cdot\dfrac{\partial\phi}{\partial\boldsymbol{\tau}_{\mathrm{R}}}} \tag{2.60}$$

is obtained analogously to eqns (2.49) and (2.50). The latter back-rotated configuration enables a plane stress description of the material in arbitrarily shaped shells using tensors in Cartesian components that refer to local, material-attached Cartesian coordinate systems. Furthermore, in this case the rate-type equations, e.g. for $\dot{\boldsymbol{\tau}}_{\mathrm{R}}$ and the elastic–plastic tangent operator $\mathbb{C}^{\mathrm{ep}}_{\mathrm{R}}$ become formally identical to the expressions of the theory of small strains.

In the formulation of the virtual work principle and in the stiffness matrix we have applied the

second Piola–Kirchhoff stress $\mathbf{S}_R$ corresponding to the back-rotated Kirchhoff stress $\boldsymbol{\tau}_R$. In eqn [I(2.17)] $\mathbf{S}_R$ is obtained as

$$\mathbf{S}_R = \mathbf{U}_R^{p-1}\mathbf{U}_R^{e-1}\boldsymbol{\tau}_R\mathbf{U}_R^{e-1}\mathbf{U}_R^{p-1}. \tag{2.61}$$

Its rate is then

$$\begin{aligned}\dot{\mathbf{S}}_R &= \mathbf{U}_R^{p-1}\mathbf{U}_R^{e-1}\dot{\boldsymbol{\tau}}_R\mathbf{U}_R^{e-1}\mathbf{U}_R^{p-1} + \frac{\partial}{\partial t}(\mathbf{U}_R^{p-1}\mathbf{U}_R^{e-1})\boldsymbol{\tau}_R\mathbf{U}_R^{e-1}\mathbf{U}_R^{p-1} \\ &\quad + \mathbf{U}_R^{p-1}\mathbf{U}_R^{e-1}\boldsymbol{\tau}_R\frac{\partial}{\partial t}(\mathbf{U}_R^{e-1}\mathbf{U}_R^{p-1}) \\ &= \mathbf{U}_R^{p-1}\mathbf{U}_R^{e-1}(\dot{\boldsymbol{\tau}}_R - (\mathbf{D}_R + \mathbf{W}_R^e + \mathbf{W}_R^p)\boldsymbol{\tau}_R - \boldsymbol{\tau}_R(\mathbf{D}_R - \mathbf{W}_R^e - \mathbf{W}_R^p))\mathbf{U}_R^{e-1}\mathbf{U}_R^{p-1},\end{aligned} \tag{2.62}$$

where

$$\mathbf{W}_R^e = \mathbf{Q}_R^T\mathbf{w}^e\mathbf{Q}_R = \tfrac{1}{2}(\dot{\mathbf{U}}_R^e\mathbf{U}_R^{e-1} - \mathbf{U}_R^{e-1}\dot{\mathbf{U}}_R^e) \tag{2.63}$$

and

$$\mathbf{W}_R^p = \mathbf{Q}_R^T\mathbf{w}^p\mathbf{Q}_R = \tfrac{1}{2}(\mathbf{U}_R^e\dot{\mathbf{U}}_R^p\mathbf{U}_R^{p-1}\mathbf{U}_R^{e-1} - \mathbf{U}_R^{e-1}\mathbf{U}_R^{p-1}\dot{\mathbf{U}}_R^p\mathbf{U}_R^e) \tag{2.64}$$

are the back-rotated elastic and plastic spin tensors, respectively. Equation (2.57) and (2.58) are linear relations between the components of $\mathbf{D}_R^e$, $\dot{\mathbf{U}}_R^e$ and $\mathbf{D}_R^p$, $\dot{\mathbf{U}}_R^p$. They can be solved obtaining $\dot{\mathbf{U}}_R^e$ and $\dot{\mathbf{U}}_R^p$ as linear functions of $\mathbf{D}_R^e$ and $\mathbf{D}_R^p$, From these one can compute $\mathbf{W}_R^e$ and $\mathbf{W}_R^p$. Then $\mathbf{D}_R^e$ can be obtained from eqn (2.55) as $\mathbf{D}_R^e = \mathbb{C}_R^{e-1}\cdot\mathbb{C}_R^{ep}\cdot\mathbf{D}_R$ and $\mathbf{D}_R^p$ as $\mathbf{D}_R^p = \mathbf{D}_R - \mathbf{D}_R^e$. If the elastic strains are less than about 10%, then in analogy to eqn (2.49) the approximation $\mathbb{C}_R^e \approx \mathbb{C}$ can be used and the elastic spin $\mathbf{W}_R^e$ can be omitted as well. Inserting these relations together with eqn (2.55) into eqn (2.62) and using computer algebra one obtains immediately the components of the material tensor $\hat{\mathbb{C}}_R^{ep}$ of the rate constitutive equation

$$\dot{\mathbf{S}}_R = \hat{\mathbb{C}}_R^{ep}\cdot\mathbf{D}_R. \tag{2.65}$$

The fourth-order tensor $\hat{\mathbb{C}}_R^{ep}$ does not have the usual symmetries, if the elastic strains become large: $\hat{\mathbb{C}}_{Rijkl}^{ep} \neq \hat{\mathbb{C}}_{Rklij}^{ep}$. Solving eqn $[\mathrm{I}(2.21)_1]$ with respect to $\mathbf{D}_R$ and inserting the results into eqn (2.65) (using computer algebra), one obtains the components of $\tilde{\mathbb{C}}_R^{ep}$ that appear in the rate constitutive equation

$$\dot{\mathbf{S}}_R = \tilde{\mathbb{C}}_R^{ep}\cdot\dot{\mathbf{E}}_R. \tag{2.66}$$

Again, $\tilde{\mathbb{C}}_R^{ep}$ is no longer symmetric for large elastic strains: $\tilde{\mathbb{C}}_{Rijkl}^{ep} \neq \tilde{\mathbb{C}}_{Rklij}^{ep}$. The asymmetry of the elastic–plastic tangent operator correlating the rate of the Green strains with the rate of the second Piola–Kirchhoff stresses was firstly shown for large strains in Schieck and Stumpf (1997). There it was proved furthermore, that also within the model of elastoplasticity using Lie derivatives the elastic–plastic tangent operator is non-symmetric, in general. For small elastic strains symmetry is reobtained approximately.

3. Elastic–plastic return algorithm for finite strains

In this section we will outline, how the new stress state can be obtained from the former one after a deformation increment. Furthermore, we will show which of the previous formulae have to be programmed.

Within this section the subscript old means the corresponding value obtained at the end of the converged Newton–Raphson iteration of the previous load step. Analogously, quantities without the subscript old mean the actual values in the current iteration cycle, although one does not know, whether convergence will be achieved. In the case when convergence is not yet achieved, the new values should not replace the old ones. The subscript trial refers to an assumed purely elastic incremental response. All computations are performed in the back-rotated, Lagrangian type invariant configuration $\tilde{\mathscr{B}}_*$ as depicted in Fig. 2I. Therefore, the shell theory can be formulated using plane stresses. If the shell is sufficiently thin, transverse shear stresses and strains can be neglected. The stretch in the thickness direction then depends entirely on the in-plane stretch according to the assumption of isochoric or approximately isochoric deformation as in the case of metal plasticity with small elastic strains.

The following procedure has to be evaluated in each shell layer (=integration point in the thickness direction) of the Gaussian integration points in each Newton–Raphson iteration cycle.

After the Green strain $\mathbf{E}_R$ has been determined in the material point (=layer in the Gaussian integration point) according to eqn [I(3.13)], the trial elastic Green strain $\mathbf{E}^e_{R\_trial}$ is obtained from

$$\mathbf{E}^e_{R\_trial} = \mathbf{U}^{p-1}_{R\_old}(\mathbf{E}_R - \mathbf{E}^p_{R\_old})\mathbf{U}^{p-1}_{R\_old}. \tag{3.1}$$

This equation can be derived from eqn [I(2.23)] solving it for $\mathbf{U}^e_R$ and applying the relation $\mathbf{U}^2 = \mathbf{1} + 2\mathbf{E}$.

From $\mathbf{E}^p_{R\_trial}$ the log trial strain $\mathbf{H}^e_{R\_trial}$ is determined as

$$\begin{aligned}\mathbf{H}^e_{R\_trial} &= \tfrac{1}{2}\ln(\mathbf{1} + 2\mathbf{E}^e_{R\_trial}) \\ &\approx \mathbf{E}^e_{R\_trial} - \mathbf{E}^e_{R\_trial}\mathbf{E}^e_{R\_trial} \quad (\text{if } \|\mathbf{E}^e_{R\_trial}\| < 10^{-4}).\end{aligned} \tag{3.2}$$

The application of $(3.2)_2$ for strains less than 10^{-4} ensures an accuracy of more than eight significant decimal digits. With the log (Hencky) strain the trial stress yields for Anand material [eqns (2.48), (2.60)]

$$\boldsymbol{\tau}_{R\_trial} = \mathbb{C} \cdot \mathbf{H}^e_{R\_trial}, \tag{3.3}$$

where $\mathbb{C}$ is the constant isotropic linear elasticity tensor. If, due to the yield function (2.51), $\boldsymbol{\tau}_{R\_trial}$ is in the elastic range, i.e. $\phi \leqslant 0$, no return algorithm must be performed and the actual stress $\boldsymbol{\tau}_R$ is equal to the trial stress.

If $\boldsymbol{\tau}_{R\_trial}$ lies in the inelastic range, i.e. $\phi > 0$, one has to distinguish two cases: either the previous load step has been elastic, or it has been elastoplastic. If the previous load step has been elastic, the stress $\boldsymbol{\tau}_R$ that lies on the yield surface must be determined. For moderately large elastic strains (less than about $\pm 10\%$) this can easily be done by computing the incremental trial log strain

$$\Delta\mathbf{H}^e_{R\_trial} = \mathbf{H}^e_{R\_trial} - \mathbf{H}^e_{R\_old} \tag{3.4}$$

and then determining the elastic ratio β^e such that

$$\boldsymbol{\tau}_{\mathrm{R}} = \mathbb{C} \cdot (\mathbf{H}^{\mathrm{e}}_{\mathrm{R\_old}} + \beta^{\mathrm{e}} \Delta \mathbf{H}^{\mathrm{e}}_{\mathrm{R\_trial}}) \tag{3.5}$$

satisfies the yield condition $\phi = 0$. In the case of von Mises yield condition and plane stress this is equivalent to

$$\begin{aligned}(\tau_{11}-\alpha_{11})^2 + (\tau_{22}-\alpha_{22})^2 - (\tau_{11}-\alpha_{11})(\tau_{22}-\alpha_{22}) \\ -(\tau_{11}+\tau_{22}-2\alpha_{11}-2\alpha_{22})(\alpha_{11}+\alpha_{22}) + 3(\tau_{12}-\alpha_{12})^2 - \tau_y^2 = 0,\end{aligned} \tag{3.6}$$

what leads to a quadratic equation for β^{e}. The trial incremental elastoplastic log strains then become

$$\Delta \mathbf{H}^{\mathrm{ep}}_{\mathrm{R\_trial}} = (1-\beta^{\mathrm{e}}) \Delta \mathbf{H}^{\mathrm{e}}_{\mathrm{R\_trial}}. \tag{3.7}$$

If the previous load step has been plastic, then $\beta^{\mathrm{e}} = 0$, $\Delta \mathbf{H}^{\mathrm{ep}}_{\mathrm{R\_trial}} = \Delta \mathbf{H}^{\mathrm{e}}_{\mathrm{R\_trial}}$ and the return algorithm starts with $\boldsymbol{\tau}_{\mathrm{R}} = \boldsymbol{\tau}_{\mathrm{R\_old}}$.

For very large elastic strains the outlined procedure is only a rough approximation, because then the log strains can no longer be superposed or decomposed additively (see Schieck and Stumpf, 1993), what is the basic assumption for eqn (3.4). Then the incremental trial log strain must be determined from the multiplicative decomposition

$$\mathbf{U}^{\mathrm{e2}}_{\mathrm{R\_trial}} = \exp(2\mathbf{H}^{\mathrm{e}}_{\mathrm{R\_trial}}) = \mathbf{U}^{\mathrm{e}}_{\mathrm{R\_old}} \exp(2\Delta \mathbf{H}^{\mathrm{e}}_{\mathrm{R\_trial}}) \mathbf{U}^{\mathrm{e}}_{\mathrm{R\_old}}, \tag{3.8}$$

obtained analogously to eqn [I(2.23)]. Then, however, the trail incremental elastic–plastic log strain tensor $\Delta \mathbf{H}^{\mathrm{ep}}_{\mathrm{R\_trial}}$ can be linearly separated from $\Delta \mathbf{H}^{\mathrm{e}}_{\mathrm{R\_trial}}$ according to eqn (3.7), because $\Delta \mathbf{H}^{\mathrm{e}}_{\mathrm{R\_trial}}$ and $\Delta \mathbf{H}^{\mathrm{ep}}_{\mathrm{R\_trial}}$ are coaxial having the same principal directions. But in eqn (3.5) the elastic strains resulting from $\mathbf{H}^{\mathrm{e}}_{\mathrm{R\_old}}$ and $\beta^{\mathrm{e}} \Delta \mathbf{H}^{\mathrm{e}}_{\mathrm{R\_trial}}$ must again be determined by a multiplicative superposition analogously to eqn (3.8).

The next step is to separate $\Delta \mathbf{H}^{\mathrm{ep}}_{\mathrm{R\_trial}}$ into n equal pieces of maximal moderate size, e.g.

$$\left\| \frac{1}{n} \Delta \mathbf{H}^{\mathrm{ep}}_{\mathrm{R\_trial}} \right\| \leqslant \frac{\tau_y}{10E}, \tag{3.9}$$

where τ_y is the average uniaxial yield stress and E the Young's modulus. Of course, instead of the factor 10 another sufficiently large number can be chosen. The linear separation of $\Delta \mathbf{H}^{\mathrm{ep}}_{\mathrm{R\_trial}}$ into equal pieces is exact due to their coaxiality. Then for each of the n pieces one has to determine λ such that (for $i = 0$ to $n-1$) the quantities

$$\boldsymbol{\tau}_{\mathrm{R}(i+1)} := \boldsymbol{\tau}_{\mathrm{R}(i)} + \mathbb{C}^{\mathrm{e}}_{\mathrm{R}} \cdot \frac{1}{n} \Delta \mathbf{H}^{\mathrm{ep}}_{\mathrm{R\_trial}} - \lambda \mathbb{C}^{\mathrm{e}}_{\mathrm{R}} \cdot \frac{\partial \phi}{\partial \boldsymbol{\tau}_{\mathrm{R}(i)}}, \tag{3.10}$$

$$\boldsymbol{\alpha}_{\mathrm{R}(i+1)} := \boldsymbol{\alpha}_{\mathrm{R}(i)} + \lambda \beta h \frac{\partial \phi}{\partial \boldsymbol{\tau}_{\mathrm{R}(i)}}, \tag{3.11}$$

$$\tau_{y(i+1)} := \tau_{y(i)} + \lambda \sqrt{\tfrac{3}{2}} (1-\beta) h \tag{3.12}$$

satisfy the yield condition $\phi = 0$ with β and h given in eqns (2.52) and (2.53). For the von Mises yield condition and plane stresses this is equivalent to eqn (3.6), what yields a quadratic equation for λ.

If in the actual Newton–Raphson iteration cycle no convergence is obtained, all quantities with the subscript old must be kept and the values for $\boldsymbol{\alpha}_R$ and τ_y must be reset to the values from the end of the previous converged load step.

If with the actual Newton–Raphson iteration cycle convergence is achieved, $\mathbf{H}^e_{R\_old}$, $\mathbf{U}^p_{R\_old}$ and $\mathbf{E}^p_{R\_old}$ have to be updated as follows:

$$\mathbf{H}^e_{R\_old} := \mathbf{H}^e_R, \quad \mathbf{U}^p_{R\_old} := \mathbf{U}^p_R, \quad \mathbf{E}^p_{R\_old} := \mathbf{E}^p_R. \tag{3.13}$$

From eqn (3.3) one gets

$$\mathbf{H}^e_R = \mathbb{C}^{-1} \cdot \boldsymbol{\tau}_R. \tag{3.14}$$

$\mathbf{U}^p_R$ is obtained by introducing eqn [I(2.23)] into $\mathbf{U}^e_R \mathbf{U}^2_R \mathbf{U}^e_R$, yielding

$$\mathbf{U}^e_R \mathbf{U}^2_R \mathbf{U}^e_R = \mathbf{U}^e_R \mathbf{U}^p_R \mathbf{U}^{e2}_R \mathbf{U}^p_R \mathbf{U}^e_R = (\mathbf{U}^e_R \mathbf{U}^p_R \mathbf{U}^e_R)^2, \tag{3.15}$$

where $\mathbf{U}^e_R = \exp \mathbf{H}^e_R$ and $\mathbf{U}^2_R = (\mathbf{1} + 2\mathbf{E}_R)$ is computed from $\mathbf{E}_R$ due to eqn [I(3.13)]. Solving eqn (3.15) for $\mathbf{U}^p_R$ we obtain

$$\mathbf{U}^p_R = \mathbf{U}^{e-1}_R \sqrt{\mathbf{U}^e_R \mathbf{U}^2_R \mathbf{U}^e_R} \mathbf{U}^{e-1}_R \tag{3.16}$$

and therefore,

$$\mathbf{E}^p_R = \tfrac{1}{2}(\mathbf{U}^{p2}_R - \mathbf{1}). \tag{3.17}$$

Since all tensors refer to the material-attached Cartesian reference frame (and therefore have Cartesian components), all numerical tensor computations in the finite element code can be performed easily as standard matrix calculations.

4. Numerical implementation

In Part I an eight-node quadrilateral arbitrarily shaped shell element with nodes at the corners and at the mid-points of the edges has been developed. Each node has three displacement degrees-of-freedom and three director-difference degrees-of-freedom. The corresponding shape functions are the usual Lagrange interpolation polynomials. They are complete up to the second-order with incomplete contributions of the third-order. The same shape functions are used for the Lagrange multiplier field η that controls the director length. If η is not condensed, its nodal degree-of-freedom is added to each node as seventh degree-of-freedom. If η is condensed on element level, only bi-linear shape functions with four degrees-of-freedom are used in combination with an additional stabilization energy $W_{\text{gradthick}}$ according to Section 5I. The trial functions for the two components of the Lagrange multiplier field $\boldsymbol{\lambda} = (\lambda_1, \lambda_2)$ are bi-linear with four degrees-of-freedom for each component. If these degrees-of-freedom are not condensed in the element routine, they are not added as eighth and ninth degree-of-freedom to the corner-nodes as it would correspond to their physical meaning. They are added as eighth and ninth degree-of-freedom to the mid-nodes in such a manner that λ_1 is continuous in the local material-attached X^2-direction and that λ_2 is continuous in the local material-attached X^1-direction. The reason for this unusual implementation is described in Section 5I.

The element routine for the element residual force vector RFV and the element stiffness matrix STM is divided into nine steps described below. The integration over the element mid-surface is performed using nine-point Gaussian quadrature and is carried out in the fictitious flat reference configuration $\mathscr{B}_*$ described in Section 2I. This means that the coordinates X^1 and X^2 (see Section 3I) can be chosen as the local convective element coordinates and have fixed boundaries in each element, e.g. $(X^1, X^2) \in [-1, 1] \times [-1, 1]$.

The first step is to compute $\boldsymbol{\gamma}_R$ and $\boldsymbol{\chi}_R$ in each Gaussian integration point according to Section 3I. There, $\mathbf{v}$ is the three-dimensional mid-surface displacement vector and ∇ means the gradient with respect to the X^1, X^2 coordinates of the fictitious reference configuration, i.e. the element coordinates. The values of the components of $\mathbf{v}$ have to be interpolated from the nodal values using the above mentioned shape functions. On the strain field $\boldsymbol{\gamma}$ according to eqn [I(3.14)$_2$] the assumed strain procedure due to Section 6I, or due to another proposed procedure, e.g. according to Bathe and Dvorkin (1986), has to be applied. In eqn [I(3.15)] $(\mathbf{t}-\mathbf{t}_0)$ is the three-dimensional director-difference vector. $\mathbf{U}^f_{(0)}$ is the fictitious 2×2 membrane stretch tensor due to the mapping from the fictitious flat reference configuration into the real undeformed configuration of the shell. It can be obtained according to eqn [I(3.16)]. $\mathbf{U}^f_{(1)}$, also a 2×2 tensor, has to be obtained from eqn [I(3.17)]. Both tensors, $\mathbf{U}^f_{(0)}$ and $\mathbf{U}^f_{(1)}$, may be stored permanently for each integration point of each element in order to avoid their repeated computation. Using computer algebra it is easy to generate a highly efficient program code for computing $\boldsymbol{\gamma}_R$ and $\boldsymbol{\chi}_R$.

In the second step, the back-rotated Kirchhoff stress $\boldsymbol{\tau}_R$ has to be computed in each integration point in the thickness direction over each Gaussian mid-surface integration point. For elastoplastic computations seven layers are used normally, while in the case of pure elasticity two or three layers are expected to be sufficient. The positions of the thickness integration points are given by coordinates $\zeta \in [-H/2, H/2]$, where H is the reference thickness given by $H = h_0/|\mathbf{t}_0|$ with h_0 and $|\mathbf{t}_0|$ as the thickness and the director length in the undeformed configuration, respectively. The director length in the undeformed configuration is determined by the isochoric constraint of the mapping from the fictitious flat reference configuration into the undeformed one. This implies the condition $\det(\mathbf{U}^f_{(0)})|\mathbf{t}_0| = 1$. The Green strains $\mathbf{E}_R$ in the layers given by ζ are determined according to eqn [I(3.13)] as

$$\mathbf{E}_R = \boldsymbol{\gamma}_R + \zeta \boldsymbol{\chi}_R. \tag{4.1}$$

Then $\boldsymbol{\tau}_R$ can be obtained using the return algorithm described in Section 3.

In the third step, the operators $\partial \mathscr{N}_R/\partial \boldsymbol{\gamma}_R$, $\partial \mathscr{N}_R/\partial \boldsymbol{\chi}_R = \partial \mathscr{M}_R/\partial \boldsymbol{\gamma}_R$ and $\partial \mathscr{M}_R/\partial \boldsymbol{\chi}_R$ have to be determined in each Gaussian quadrature point. For this the elastic–plastic tangent modulus $\tilde{\mathbb{C}}^{ep}_R$ appearing in eqn (2.66) has to be computed, which can be obtained efficiently from $\mathbb{C}^{ep}_R$ at the end of the return algorithm, see Sections 2 and 3. Introducing eqns (2.66) and (4.1) into eqns [I(4.2)] and [I(4.3)] one obtains

$$\frac{\partial \mathscr{N}_R}{\partial \boldsymbol{\gamma}_R} = \int_{-H/2}^{H/2} \tilde{\mathbb{C}}^{ep}_R \, d\zeta, \tag{4.2}$$

$$\frac{\partial \mathscr{N}_R}{\partial \boldsymbol{\chi}_R} = \frac{\partial \mathscr{M}_R}{\partial \boldsymbol{\gamma}_R} = \int_{-H/2}^{H/2} \tilde{\mathbb{C}}^{ep}_R \zeta \, d\zeta, \tag{4.3}$$

$$\frac{\partial \mathscr{M}_R}{\partial \boldsymbol{\chi}_R} = \int_{-H/2}^{H/2} \tilde{\mathbb{C}}_R^{ep} \zeta^2 \, d\zeta. \tag{4.4}$$

The integration is performed numerically using the ζ-coordinates of the layers as integration points.

The fourth step is to calculate the stress resultants and stress couples $\mathscr{N}_R$ and $\mathscr{M}_R$ in each Gaussian quadrature point from the Kirchhoff stress $\mathbf{S}_R$ according to eqns [I(4.2)] and [I(4.3)]. $\mathbf{S}_R$ can be obtained from $\boldsymbol{\tau}_R$ at the end of the return algorithm (Section 3) using eqn (2.61). Analogously to the previous step, the integration over the thickness is performed numerically using the ζ-coordinates of the layers as integration points.

In the fifth step, the virtual membrane strains $\delta_i \boldsymbol{\gamma}_R$ and the virtual bending strains $\delta_i \boldsymbol{\chi}_R$ have to be determined in each Gaussian quadrature point. Here $\delta_i(\,)$ denotes the variation of $(\,)$ due to the variation of the i-th degree-of-freedom. The formulae for $\delta_i \boldsymbol{\gamma}_R$ and $\delta_i \boldsymbol{\chi}_R$ can be obtained from eqns [I(3.18)] and [I(3.19)] by replacing the variation symbol δ by δ_i. Then $\delta_i \mathbf{v}$ contains the shape functions for the components of the displacement vector $\mathbf{v}$ due to the i-th degree-of-freedom in the element, where $\delta_i \nabla \mathbf{v}$ is its gradient. The meaning of $\delta_i \mathbf{t}$ and $\delta_i \nabla \mathbf{t}$ is analogous to those of $\delta_i \mathbf{v}$ and $\delta_i \nabla \mathbf{v}$, where $\delta_i \mathbf{t} \equiv \delta_i(\mathbf{t} - \mathbf{t}_0)$ contains the shape function for the components of the director-differences due to the i-th degree-of-freedom in the element. Within this computation step one should not forget to apply the assumed strain procedure of Section 6I to $\delta_i \boldsymbol{\gamma}$ of eqn [I(3.18)$_2$]. The same procedure as for $\boldsymbol{\gamma}$ in the first step of the element routine should be applied.

The sixth step is the assemblage of the components RFV_i of the element residual force vector RFV,

$$\begin{aligned} RFV_i = \int_A \{ & \mathscr{N}_R \cdot \delta_i \boldsymbol{\gamma}_R + \mathscr{M}_R \cdot \delta_i \boldsymbol{\chi}_R - \mathbf{P} \cdot \delta_i \mathbf{v} + (\mathbf{t}\mathbf{F}_{*|\zeta=0} - \mathbf{t}_0 \mathbf{F}^{f}_{|\zeta=0}) \cdot \delta_i \boldsymbol{\lambda} + \mathbf{t} \cdot \delta_i \nabla \mathbf{v} \boldsymbol{\lambda} + \delta_i \mathbf{m} \cdot \mathbf{F}_{*|\zeta=0} \boldsymbol{\lambda} \\ & + \delta_i \eta (\det \mathbf{F}^{(3\times 3)}_{*|\zeta=0} - \det \mathbf{F}^{f(3\times 3)}_{|\zeta=0}) + \eta \operatorname{tr}(\delta_i \mathbf{F}^{(3\times 3)}_{*|\zeta=0} \mathbf{F}^{(3\times 3)-1}_{*|\zeta=0}) \det \mathbf{F}^{(3\times 3)}_{*|\zeta=0} \} \, dA, \end{aligned} \tag{4.5}$$

where the integration over the area A of the element is performed in the fictitious flat reference configuration $\mathscr{B}_*$, and $\mathbf{P}$ denotes the vector of dead loads per unit area of the mid-surface in this configuration.

The first line in eqn (4.5) is due to the internal virtual work IVW eqn [I(4.4)$_2$] and dead loading. The second, third and fourth lines are due to the extension terms XVW in the virtual work principle as they are established in eqn [I(4.5)], where also the meaning of $\mathbf{F}_{*|\zeta=0}$, $\mathbf{F}^{f}_{|\zeta=0}$, $\mathbf{F}^{(3\times 3)}_{*|\zeta=0}$ and $\mathbf{F}^{f(3\times 3)}_{|\zeta=0}$ are explained in detail. In analogy to step five, here $\delta_i(\,)$ means the variation of $(\,)$ due to the variation of the i-th degree-of-freedom in the element. Thus, $\delta_i \boldsymbol{\lambda}$ and $\delta_i \eta$ are the shape functions for $\boldsymbol{\lambda}$ and η associated with the i-th degree-of-freedom. If the i-th degree-of-freedom does not correspond to $\boldsymbol{\lambda}$ or η, then $\delta_i \boldsymbol{\lambda}$ and $\delta_i \eta$, respectively, are zero. In the case of the condensation of the degrees-of-freedom of the Lagrange multipliers $\boldsymbol{\lambda}$ and η, one must add $-\delta_i W_{shear}$ and $-\delta_i W_{bulk}$ to RFV_i with W_{shear} and W_{bulk} due to Section 4I, e.g.

$$RFV_i := RFV_i - \int_A \left\{ \frac{1.2}{GH} \boldsymbol{\lambda} \cdot \mathbf{U}^{f2}_{(0)} \delta_i \boldsymbol{\lambda} |\mathbf{t}_0|^2 + \frac{\eta}{E_b H} \delta_i \eta \right\} dA. \tag{4.6}$$

For pressure loads p per unit area of the actual mid-surface and the terms corresponding to eqn [I(4.19)] must be added to RFV_i, replacing there $\delta \mathbf{v}$ by $\delta_i \mathbf{v}$:

$$RFV_i := RFV_i + \int_A p \left(\left.\frac{\partial \mathbf{x}}{\partial X^1}\right|_{\zeta=0} \times \left.\frac{\partial \mathbf{x}}{\partial X^2}\right|_{\zeta=0} \right) \cdot \delta_i \mathbf{v} \, \mathrm{d}A, \tag{4.7}$$

where $\partial \mathbf{x}/\partial X^1{}_{|\zeta=0}$ and $\partial \mathbf{x}/\partial X^2{}_{|\zeta=0}$ are the actual convective tangent vectors, which can be found in the first two columns of $\mathbf{F}_{*|\zeta=0}$ (see Section 5I).

In step seven, the material part of the stiffness matrix STM due to the material part of the incremental virtual work ΔIVW {eqn [I(4.12)]} is established as

$$STM_{ij} = \int_A \left\{ \delta_i \boldsymbol{\gamma}_\mathrm{R} \cdot \left(\frac{\partial \mathscr{N}_\mathrm{R}}{\partial \boldsymbol{\gamma}_\mathrm{R}} \cdot \delta_j \boldsymbol{\gamma}_\mathrm{R} + \frac{\partial \mathscr{N}_\mathrm{R}}{\partial \boldsymbol{\chi}_\mathrm{R}} \cdot \delta_j \boldsymbol{\chi}_\mathrm{R} \right) + \delta_i \boldsymbol{\chi}_\mathrm{R} \cdot \left(\frac{\partial \mathscr{M}_\mathrm{R}}{\partial \boldsymbol{\gamma}_\mathrm{R}} \cdot \delta_j \boldsymbol{\gamma}_\mathrm{R} + \frac{\partial \mathscr{M}_\mathrm{R}}{\partial \boldsymbol{\chi}_\mathrm{R}} \cdot \delta_j \boldsymbol{\chi}_\mathrm{R} \right) \right\} \mathrm{d}A. \tag{4.8}$$

Since, according to Section 2, $\tilde{\mathbb{C}}^{\mathrm{ep}}_\mathrm{R}$ is not symmetric, also the operators $\partial \mathscr{N}_\mathrm{R}/\partial \boldsymbol{\gamma}_\mathrm{R}$, $\partial \mathscr{N}_\mathrm{R}/\partial \boldsymbol{\chi}_\mathrm{R} = \partial \mathscr{M}_\mathrm{R}/\partial \boldsymbol{\gamma}_\mathrm{R}$ and $\partial \mathscr{M}_\mathrm{R}/\partial \boldsymbol{\chi}_\mathrm{R}$ [see eqns (4.2)–(4.4)] are not symmetric and therefore, the stiffness matrix is not symmetric as well. Only for small elastic strains the symmetry of these operators is achieved (see also Schieck and Stumpf, 1997).

In the eighth step, the geometric part of the stiffness matrix is added. For this purpose $\delta_i \delta_j \boldsymbol{\gamma}_\mathrm{R}$ and $\delta_i \delta_j \boldsymbol{\chi}_\mathrm{R}$ must be determined in each Gaussian integration point. This can be performed in analogy to the computation of $\delta_i \boldsymbol{\gamma}_\mathrm{R}$ and $\delta_i \boldsymbol{\chi}_\mathrm{R}$ in the fifth step, starting with eqns [I(3.20)] and [I(3.21)] and replacing there the symbols δ and Δ by δ_i and δ_j, respectively. Again, one has to apply the assumed strain method of Section 6I, also to $\delta_i \delta_j \boldsymbol{\gamma}$ according to eqn [I(3.20)$_2$]. It must be the same procedure as for $\boldsymbol{\gamma}$ and $\delta_i \boldsymbol{\gamma}$. The geometrical part of the incremental virtual work ΔIVW {eqn [I(4.12)]} is then added as

$$STM_{ij} := STM_{ij} + \int_A \{ \mathscr{N}_\mathrm{R} \cdot \delta_i \delta_j \boldsymbol{\gamma}_\mathrm{R} + \mathscr{M}_\mathrm{R} \cdot \delta_i \delta_j \boldsymbol{\chi}_\mathrm{R} \} \, \mathrm{d}A. \tag{4.9}$$

This contribution is symmetric. For pressure loads the expression

$$STM_{ij} := STM_{ij} + \int_A p \left(\frac{\partial \delta_j \mathbf{v}}{\partial X^1} \times \left.\frac{\partial \mathbf{x}}{\partial X^2}\right|_{\zeta=0} + \left.\frac{\partial \mathbf{x}}{\partial X^1}\right|_{\zeta=0} \times \frac{\partial \delta_j \mathbf{v}}{\partial X^2} \right) \cdot \delta_i \mathbf{v} \, \mathrm{d}A \tag{4.10}$$

has to be introduced, which is not symmetric. Only for suitable boundary conditions there exists a potential for the pressure load, and then the asymmetries of eqn (4.10) vanish in the global stiffness matrix. This then allows one to symmetrize the contributions of the pressure loads to the element stiffness matrix. The expressions for $\partial \delta_j \mathbf{v}/\partial X^1$ and $\partial \delta_j \mathbf{v}/\partial X^2$ can be obtained from the first two columns of $\delta_j \mathbf{F}_{*|\zeta=0}$. They are the variations of $\mathbf{F}_{*|\zeta=0}$ due to the variation of the j-th displacement degree-of-freedom in the element.

The ninth and last step consists of adding the contributions from the extension terms ΔXVW of the incremental virtual work {eqn [I(4.13)]} to the stiffness matrix. These terms correspond to the terms 4–8 of eqn (4.5) and are derived from eqn [I(4.13)] as

$$STM_{ij} := STM_{ij} + \int_A \{ (\delta_j \mathbf{t} \mathbf{F}_{*|\zeta=0} + \mathbf{t} \delta_j \nabla \mathbf{v}) \cdot \delta_i \boldsymbol{\lambda}$$

$$+(\delta_i \mathbf{t}\mathbf{F}_{*|\zeta=0}+\mathbf{t}\delta_i\nabla\mathbf{v})\cdot\delta_j\boldsymbol{\lambda}+(\delta_j\mathbf{t}\delta_i\nabla\mathbf{v}+\delta_i\mathbf{t}\delta_j\nabla\mathbf{v})\cdot\boldsymbol{\lambda}$$
$$+[\delta_i\eta\,\mathrm{tr}(\delta_j\mathbf{F}^{(3\times3)}_{*|\zeta=0}\mathbf{F}^{(3\times3)-1}_{*|\zeta=0})+\delta_j\eta\,\mathrm{tr}(\delta_i\mathbf{F}^{(3\times3)}_{*|\zeta=0}\mathbf{F}^{(3\times3)-1}_{*|\zeta=0})]\det\mathbf{F}^{(3\times3)}_{*|\zeta=0}$$
$$+\eta[\mathrm{tr}(\delta_i\mathbf{F}^{(3\times3)}_{*|\zeta=0}\mathbf{F}^{(3\times3)-1}_{*|\zeta=0})\,\mathrm{tr}(\delta_j\mathbf{F}^{(3\times3)}_{*|\zeta=0}\mathbf{F}^{(3\times3)-1}_{*|\zeta=0})$$
$$-\mathrm{tr}(\delta_i\mathbf{F}^{(3\times3)}_{*|\zeta=0}\mathbf{F}^{(3\times3)-1}_{*|\zeta=0}\delta_j\mathbf{F}^{(3\times3)}_{*|\zeta=0}\mathbf{F}^{(3\times3)-1}_{*|\zeta=0})\det\mathbf{F}^{(3\times3)}_{*|\zeta=0}]\}\,\mathrm{d}A. \tag{4.11}$$

If the contributions due to eqn (4.6) are added to the residual force vector, the expression

$$STM_{ij} := STM_{ij}-\int_A\left\{\frac{1.2}{GH}\delta_j\boldsymbol{\lambda}\cdot\mathbf{U}^{\mathrm{f2}}_{(0)}\delta_i\boldsymbol{\lambda}|\mathbf{t}_0|^2+\frac{1}{E_{\mathrm{b}}H}\delta_j\eta\delta_i\eta\right\}\mathrm{d}A \tag{4.12}$$

must be introduced into the stiffness matrix in order to enable the condensation of the Lagrange multipliers $\boldsymbol{\lambda}$ and η.

5. Numerical examples

Convergence tests within the linear and nonlinear solutions performed with the presented finite element have already been discussed in Part I. For this purpose the hemispherical shells already calculated by MacNeal and Harder (1985) and Simo et al. (1990) have been analyzed. It was shown that the element performs well. The application of our proposed assumed strain method 2 has shown better results for coarse meshes than the assumed strain methods of Bathe and Dvorkin (1986), Huang and Hinton (1986) and Huang (1987a, b).

5.1. Elastic–plastic tension of a strip

As first example the elastic–plastic tension of the strip recently investigated by Miehe (1998b) is analyzed. The geometry is given by the length $L = 17.78$ mm, the width $B = 13.545$ mm and the thickness $H = 1.0$ mm. As a small imperfection the width in the middle of the strip is reduced by 0.0225 mm at both sides. Due to the symmetry only a quarter of the specimen is discretized. The material is characterized by a saturation-type isotropic hardening model with a yield stress according to the function

$$\tau_y = \tau_{y0}+h\varepsilon_{\mathrm{p}}+(y_\infty-\tau_{y0})(1-\exp(-\eta\varepsilon_{\mathrm{p}})) \tag{5.1}$$

where

$$\varepsilon_{\mathrm{p}} = \sqrt{\frac{2}{3}}\int_t\dot{\lambda}\,\mathrm{d}t \tag{5.2}$$

is the integrated plastic equivalent strain with $\dot{\lambda}$ according to eqn (2.34). The material constants

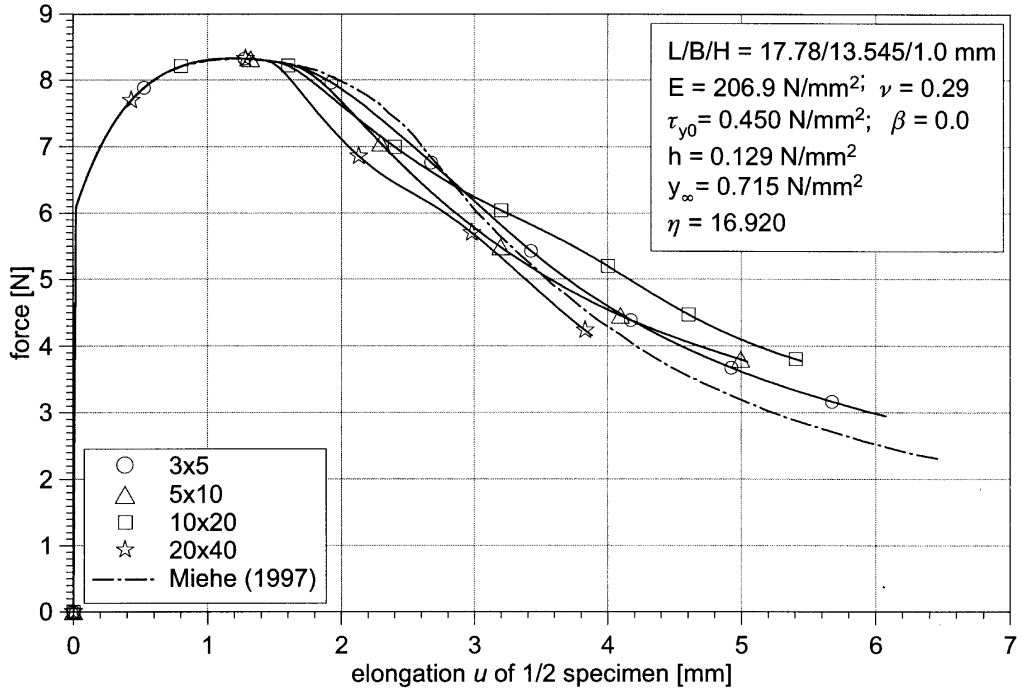

Fig. 1. Elastic–plastic tension of a strip with symmetric width reduction as imperfection.

and the load–deformation curves for various regular meshes are presented in Fig. 1 and the corresponding deformation modes are shown in Fig. 2. One can easily recognize the shear-band-like localizations of the deformation, which were obtained for sufficiently fine meshes. The shear-bands always begin at the locations of the imperfections and have an inclination of about 55°. Because of the symmetry of the imperfections on both sides of the specimen the shear-bands form a double-cross. Miehe (1998b) used a 10×20 mesh with brick-type eight-node shell elements without obtaining shear-bands. Such an element is equivalent to a four-node quadrilateral shell element, which typically represents only an incomplete linear (i.e. mainly constant) deformation mode. The eight-node shell element of the present paper can describe complete bi-linear deformation modes with some quadratic enrichments and therefore it produces better approximations, in general.

In Figs 3 and 4 the load–deformation curve and the deformation modes are shown for the same sample with a thickness reduction of 5% for the element in the center as imperfection instead of the width reduction. For the material with nonlinear hardening as in Fig. 1 only a double shear-band evolves. For material with constant hardening $E_T = 0.5$ MPa (which is approximately the E_T of the nonlinear hardening material for $\varepsilon_p = 15\%$) only a diffuse necking occurs (Fig. 4).

The macro shear-bands of Figs 2 and 4 can be observed in strip tension experiments and are triggered by a small imperfection in combination with decreasing plastic hardening. They can be analyzed also by admitting weak discontinuities of the plastic deformation rate on singular lines and deriving the acoustic tensor (see e.g. Le et al., 1998). Points suffering a little bit more

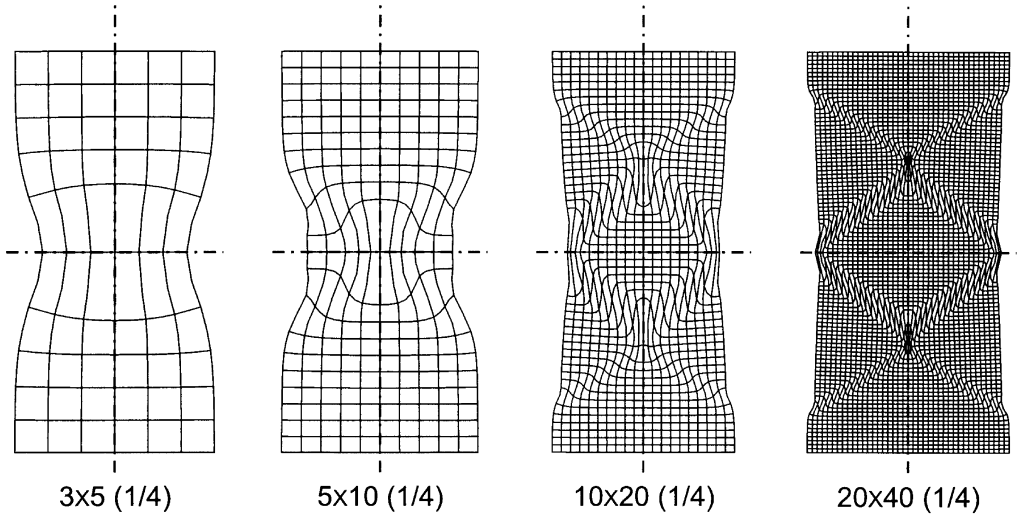

Fig. 2. Tension of a strip with symmetric width reduction as imperfection: deformations at about $u = 4$ mm elongation for half specimen.

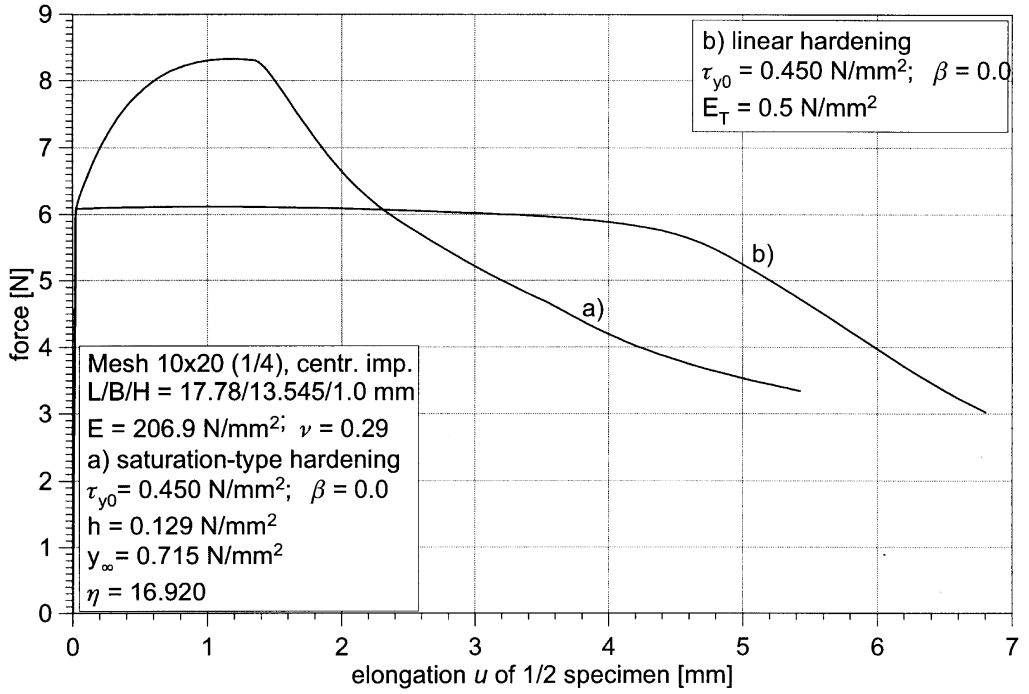

Fig. 3. Elastic–plastic tension of a strip with central imperfection: (a) saturation-type hardening; (b) linear hardening.

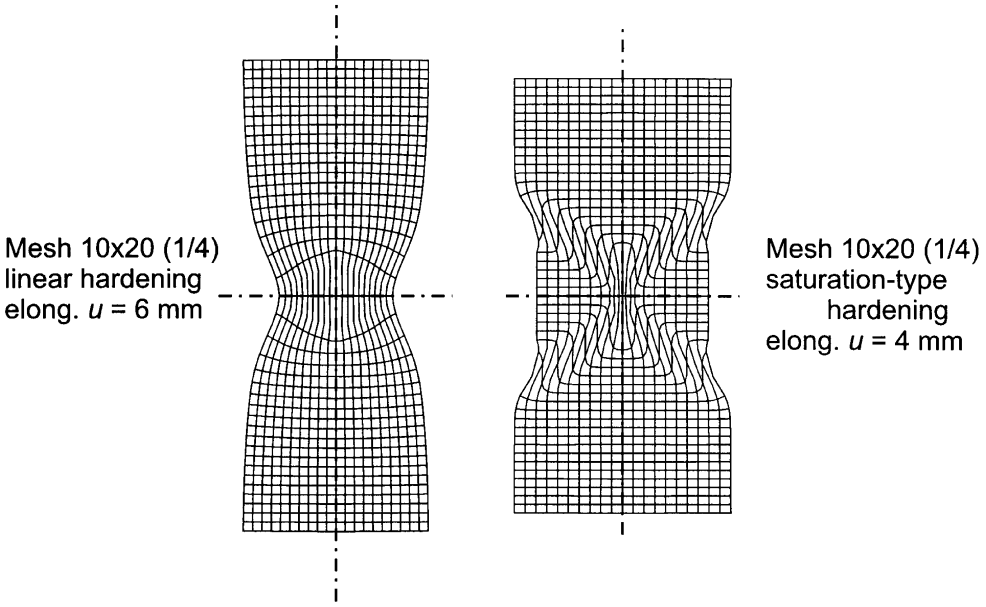

Fig. 4. Elastic–plastic tension of a strip with central imperfection: deformations for linear and saturation-type hardening.

plastification than their neighboring points react weaker than their surrounding. This effect grows rapidly with increasing plastic deformation and enables then the formation of macro shear-bands. Therefore, the specimen with constant hardening does not develop macro shear-bands.

5.2. *Elastic–plastic deflection of a square plate*

Next we consider the elastoplastic deformation of the dead-loaded, simply supported thin square plate investigated by Büchter et al. (1994) and Miehe (1998b). The plate has an edge length of 508 mm and a thickness of 2.54 mm. The coefficients of the ideal plastic material, the load–deflection curves for various meshes without and with adaptation (A) and the final deformation picture are presented in Fig. 5. Up to a deformation of 22 mm all solutions coincide. For further increasing deformations folds develop at the corners that require more refined meshes. With a uniform 24×24 mesh or a non-uniform 16×16 discretization mesh convergence is obtained.

5.3. *Scordelis-Lo roof*

The Scordelis-Lo roof is a frequently used sensitive benchmark problem for shell elements. Recently, Roehl and Ramm (1996) and Brank et al. (1997) presented interesting new results for this elastic–plastic buckling problem and its post-buckling behavior. Although this example accounts only for small strains it is analyzed here to check the performance of our proposed eight-node shell element. Material data, geometry, reference load and boundary conditions are given in Fig. 6. According to the symmetry, only a quarter of the shell is discretized. The results of our computations are depicted in Figs 6 and 7, and they are compared with those of the above

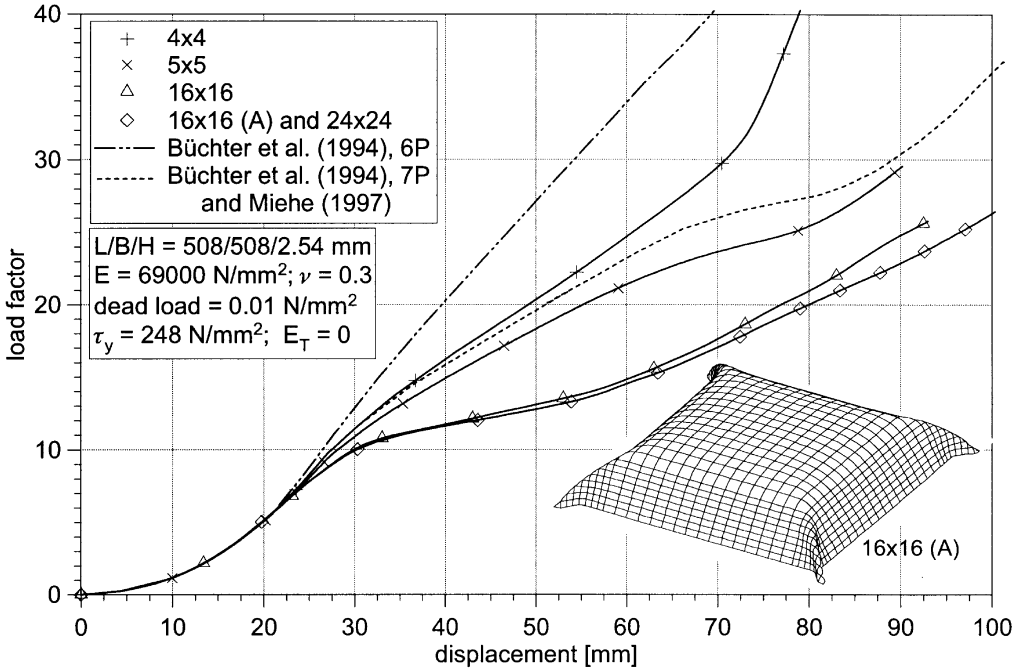

Fig. 5. Simply supported, dead-loaded square plate.

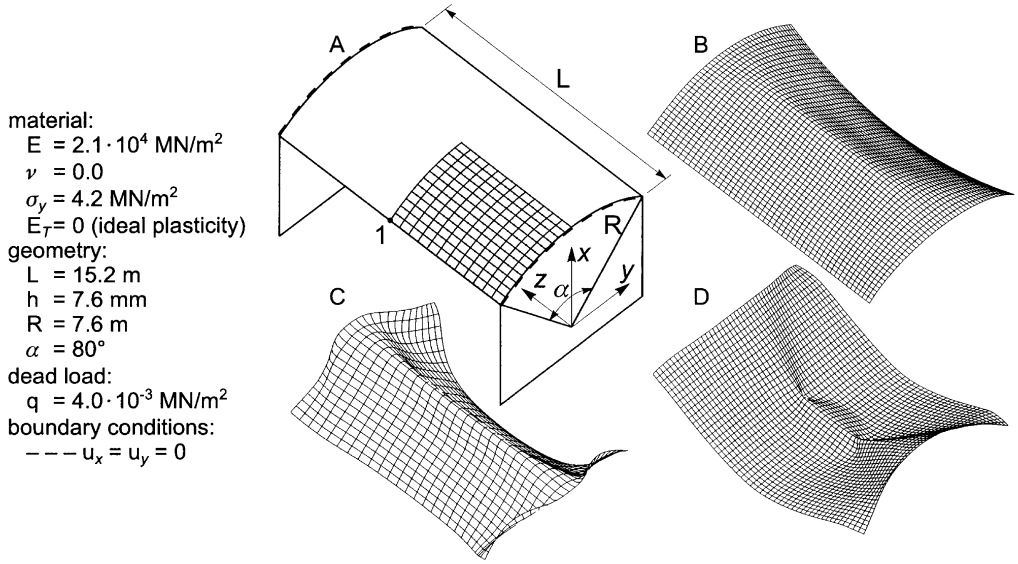

Fig. 6. Scordelis-Lo roof: geometry, material, load, boundary condition and deformation modes.

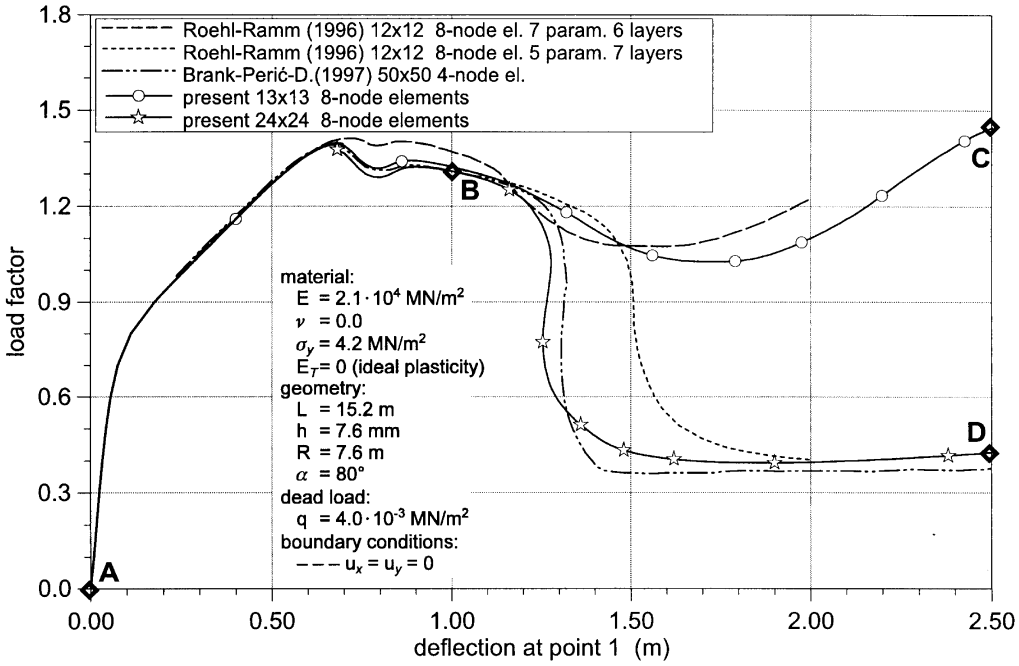

Fig. 7. Scordelis-Lo roof: deflections at point 1 on the free edge.

mentioned authors. Roehl and Ramm (1996) applied various continuum and shell elements, where the continuum and most of their shell elements led to the deformation mode C, while they obtained deformation mode D with a 5-P model (7 PSI). With our eight-node shell element we have obtained the buckling mode D for a sufficiently fine element grid. A 13×13 or more coarse discretization produces the 'folded' mode C, while a 14×14 or finer mesh yields the 'double wrinkled' mode D. Further mesh refinement, e.g. 24×24 eight-node elements of the present paper, confirms the result of Brank et al. (1997) obtained by 50×50 four-node elements. Obviously, the 12×12 discretization of Roehl and Ramm (1996) using their four-node seven-parameter shell element is too coarse, however, in combination with their eight-node five-parameter element it is fine enough to produce the solution with the 'double wrinkled' mode D.

5.4. *Fixed-end torsion of a moderately thick cylinder*

The next example discussed here is the fixed-end torsion of a moderately thick cylindrical shell with large strain elastic–plastic deformations (Fig. 8). Length L and radius R of the cylinder are chosen to be equal and the thickness H is 10% of the radius. One end of the cylinder is clamped. The other end, which is twisted, is stiffened by a ring with a length of $L/8$, with a thickness of $2H$ and with a Young's modulus of 100 times the Young's modulus E of the shell material and with infinite yield stress. Additionally, the rotations around the peripherical line of the ring and its displacement in the axial direction are suppressed. In Fig. 8 the buckled cylinder and the corresponding dimensionless load–displacement curves are plotted for different ratios β of kinematic

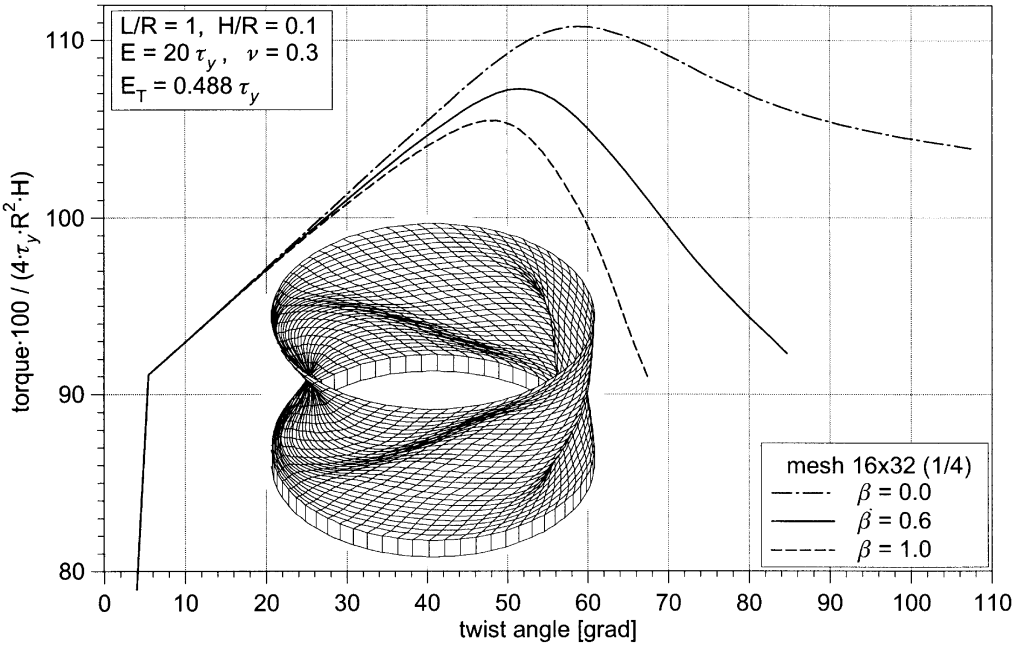

Fig. 8. Fixed-end torsion of a cylinder: buckled shell and load–displacement curves for different ratios β for kinematic to isotropic hardening.

to isotropic hardening for the given material with $E = 20\tau_y$, where τ_y is the initial uniaxial yield stress and with $E_T = 0.488\tau_y$ as a plastic tangent modulus. The first kink in the curves of Fig. 8 is due to the appearance of yielding and the next kinks result from plastic buckling. One can clearly recognize the influence of the kinematic hardening ratio β on the buckling load and on the post-buckling behavior.

The torque has been applied by one force vector for each quarter of the cylinder acting in a tangent direction on the stiffened ring. The buckling modes have been calculated without the help of additionally introduced imperfections. By a coarse calculation for the whole cylinder it has been checked first that for the given geometry only four buckling waves occur. Then a detailed refined analysis has been performed only for a quarter of the cylinder periphery using appropriate coupling conditions at the sides. Therefore, the meshes indicated in Figs 8 and 9 refer to a quarter of the cylinder. Due to the low ratio of E/τ_y the elastic strains are moderately large here. The plastic strains become really very large due to the large angle of twist.

In Fig. 9 the mesh convergence is tested for $\beta = 0.6$. One can see that eight elements for a quarter of the circumflex are enough, but that a mesh refinement in the length direction increases the accuracy. However, in the post-buckling range even the 8×8 mesh is only about 5% stiffer than the 16×32 mesh. Concerning the maximum load, the differences are much smaller. For $\beta = 0$ and $\beta = 1$ the behavior is similar.

In the far post-buckling range of deformation frequently 'plastic oscillations' occurred during the Newton–Raphson iterations. This fact results from an unstable chaotic behavior of the iterations induced by the switch of integration points between plastic and elastic behavior. Applying

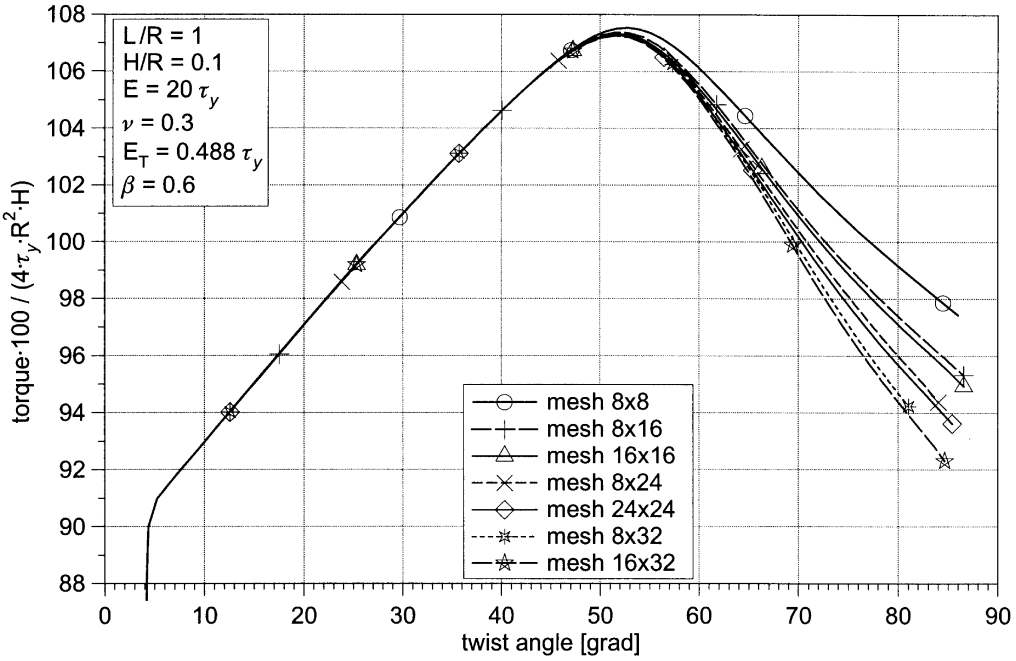

Fig. 9. Fixed-end torsion of a cylinder; mesh convergence.

a reasonable damping factor the oscillations can be suppressed for a large range of deformation allowing to keep the relative norm of the increments in the convergence condition near 10^{-3}. The relative norm is related to the Euclidean norm of the first increment in a new load–displacement step.

Figure 10 presents the load–displacement curves for the same material but with other Young's moduli, ranging from 2.5 times the initial yield stress ($E = 2.5\tau_y$) to 1000 times ($E = 1000\tau_y$) like it is typical for metal plasticity. In order to restrict the computational demand, only an 8×8 mesh for a quarter of the cylinder was applied. According to the previous investigations (see Fig. 9) the maximum loads are predicted nearly exactly and in the post-buckling range the expected differences in the loads are less than 5%.

In the case of a very weak material with $E = 2.5\tau_y$ the buckling occurs before yielding. This can be recognized by the smooth divergence of the elastic–plastic solution from the purely elastic one. For $E = 5\tau_y$ buckling and plastification occur simultaneously, which can be seen by the strong kink in the elastic–plastic solution and the weak kink between the elastic pre-buckling solution and the continuation of the purely elastic load path. In the regions, where the load increases with the deformation, the buckling waves have always very small amplitudes. After reaching the maximum load the buckling waves grow rapidly and become extreme. The computations were stopped, when in the trial deformation states during the iterations negative principal stretches occurred as a result of too strong bending inside the buckling waves.

For strong material with $E = 10\tau_y$, $E = 20\tau_y$ and $E = 1000\tau_y$ (which is typical for metal plasticity) yielding occurs before buckling. The buckling mode also evolves rather weakly at the beginning,

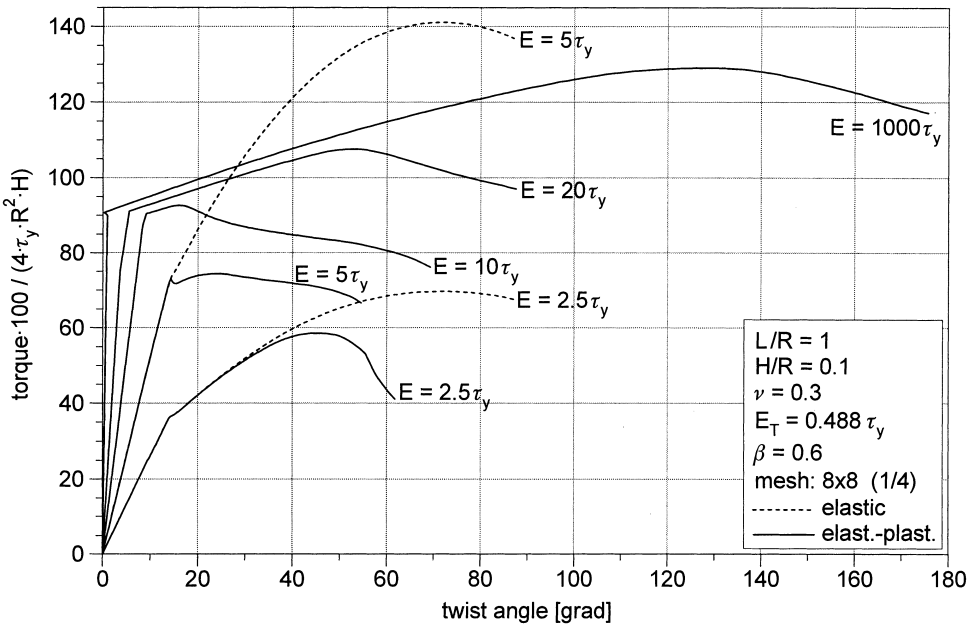

Fig. 10. Fixed-end torsion of a cylinder: influence of the ratio Young's modulus E to initial yield stress τ_y.

which can be observed only as a first smooth curvature in the previously straight load–displacement curve after the first yielding. In the regions where the load decreases with increasing deformation, the buckling waves grow rapidly and the computations were stopped during the Newton–Raphson iterations, when negative principal values of the stretches appeared.

6. Conclusions

A shell theory and an associated eight-node C^0 shell finite element for elastic–plastic material behavior are presented. The main features of the element can be briefly summarized as follows:

(1) The kinematic and constitutive concept is based on the model of finite elastoplasticity proposed in Schieck and Stumpf (1995).
(2) Reference configuration for the shell is a flat, rectangular plate allowing the application of plane stresses.
(3) The eight-node shell element has three displacement and three director degrees-of-freedom at each node, which enable us to connect easily various components of engineering structures.
(4) Elastic and plastic strains are allowed to be finite.
(5) Isotropic and kinematic hardening is taken into account.
(6) An improved assumed strain technique is proposed.

(7) To our numerical experience so far the shell element is locking-free and does not exhibit spurious modes.
(8) A wide range of numerical examples is analyzed including problems with bending strain localization and shear-band localization. The results are compared with those published in the literature, as far as such are available.
(9) The numerical examples show the good performance of the proposed shell element for the analysis of engineering structures.

Acknowledgement

The authors gratefully acknowledge financial support of the Deutsche Forschungsgemeinschaft under Contract No. ST-135/1-2.

References

Acharya, A., Shawki, T.G., 1996. The Clausius–Duhem inequality and the structure of rate-independent plasticity. Int. J. Plasticity 12 (2), 229–238.
Anand, L., 1979. On H. Hencky's approximate strain-energy function for moderate deformations. Trans. ASME, J. Appl. Mech. 76, 78–82.
Anand, L., 1986. Moderate deformations in extension–torsion of incompressible isotropic elastic materials. J. Mech. Phys. Solids 34 (3) 293–304.
Bathe, K.J., Dvorkin, E.N., 1986. A formulation of general shell elements, the use of mixed interpolation of tensorial components. Int. J. Num. Meth. Engng 22, 697–722.
Brank, B., Peric, D., Damjanic, F., 1997. On large deformations of thin elasto-plastic shells: implementation of a finite rotation model for quadrilateral shell element. Int. J. Num. Meth. Engng 40, 689–726.
Büchter, N., Ramm, E., Roehl, D., 1994. Three-dimensional extension of non-linear shell formulation based on the enhanced assumed strain concept. Int. J. Num. Meth. Engng 37, 2551–2568.
Huang, H.C., 1987a. Implementation of assumed strain degenerated shell elements. Comp. Struct. 25, 147–155.
Huang, H.C., 1987b. Membrane locking and assumed strain elements. Comp. Struct. 27, 671–677.
Huang, H.C., Hinton, E., 1986. A nine-node degenerated shell element with enhanced membrane and shear interpolation. Int. J. Num. Meth. Engng 22, 73–92.
Le, K.C., Stumpf, H., 1993. Constitutive equations for elastoplastic bodies at finite strain: thermodynamic implementation. Acta Mechanica 100, 155–170.
Le, K.C., Schütte, H., Stumpf, H., 1998. Dissipative driving force in ductile crystals and the strain localization phenomenon. Int. J. Plasticity, to appear.
MacNeal, R.H., Harder, R.L., 1985. A proposed standard set of problems to test finite element accuracy. Finite Element in Analysis and Design 1, 3–20.
Miehe, C., 1998a. A constitutive frame of elastoplasticity at large strains based on the notion of a plastic metric. Int. J. Solids Structures 35 (30), 3859–3897.
Miehe, C., 1998b. A theoretical and computational model for isotropic elasto-plastic stress analysis in shells at large strains. Comp. Meth. Appl. Mech. Engng 155, 193–233.
Ogden, R.W., 1984. On Eulerian and Lagrangian objectivity in continuum mechanics. Arch. Mech. Stos. 36, 207–218.
Roehl, D., Ramm, E., 1996. Large elasto-plastic finite element analysis of solids and shells with the enhanced assumed strain concept. Int. J. Solids Structures 33 (20–22), 3215–3237.
Schieck, B., Stumpf, H., 1993. Deformation analysis for finite elastic–plastic strains in a Lagrangian-type description. Int. J. Solids Structures 30 (19), 2639–2660.

Schieck, B., Stumpf, H., 1995. The appropriate corotational rate, exact formula for the plastic spin and constitutive model for finite elastoplasticity. Int. J. Solids Structures 32 (24) 3643–3667.

Schieck, B., Stumpf, H., 1997. The asymmetry of the tangent stiffness matrix in finite elastoplasticity. ZAMM 77, T297–T298.

Sedow, L.I., 1972. A Course in Continuum Mechanics, vol. 4: Elastic and Plastic Solids and Formation of Cracks. Wolters-Noordhoff, Groningen, The Netherlands.

Simo, J.C., Rifai, M.S., Fox, D.D., 1990. On a stress resultant geometrically exact shell model. Part IV: Variable thickness shells with through the thickness stretching. Comp. Meth. Appl. Mech. Engng 81, 91–126.